

Optimal Energy Estimation in Path-Integral Monte Carlo Simulations

Wolfhard Janke^{1,2} and *Tilman Sauer*^{2,3,★}

¹ Institut für Physik, Johannes Gutenberg-Universität Mainz
55099 Mainz, Germany

email: janke@miro.physik.uni-mainz.de

² Institut für Theoretische Physik, Freie Universität Berlin
14195 Berlin, Germany

³ Max-Planck-Institut für Wissenschaftsgeschichte
Wilhelmstraße 44, 10117 Berlin, Germany

★ present address:

Institut für Wissenschaftsgeschichte, Georg-August-Universität Göttingen
Humboldtallee 11, 37073 Göttingen, Germany
email: tsauer@gwdg.de

Abstract

We investigate the properties of two standard energy estimators used in path-integral Monte Carlo simulations. By disentangling the variance of the estimators and their autocorrelation times we analyse the dependence of the performance on the update algorithm and present a detailed comparison of refined update schemes such as multi-grid and staging techniques. We show that a proper combination of the two estimators leads to a further reduction of the statistical error of the estimated energy with respect to the better of the two without extra cost.

1 Introduction

A detailed understanding of the statistical properties of many-particle quantum systems is among the most challenging objectives in condensed matter physics and physical chemistry. Apart from a few simple model systems, analytical approaches can usually only provide an approximative description whose accuracy is difficult to control inherently. Computer simulations, on the other hand, in principle yield exact results even for complicated systems such as, for example, non-linear quantum chains or quantum crystals. A combination of the two complementary approaches may thus result in valuable insights into the physics of quantum systems.

While in principle an exact method, the difficulty of computer simulations is to actually achieve the desired accuracy in practice. For path-integral Monte Carlo (PIMC) methods, which we shall consider in this paper, the draw-backs are well known.¹ Being a stochastic method, all results are subject to statistical errors which, in principle, can be made as small as desired by increasing the simulation time. The necessary discretization of the path integral, however, requires an extrapolation to the continuum limit where standard local update algorithms exhibit a severe slowing down. By this one means that successively generated paths, or more generally, configurations of a many-particle system, are highly correlated in the Monte Carlo process. This effect greatly enhances the statistical errors of the measurements in a given computer time.

More precisely the statistical uncertainty for the mean value $\overline{\mathcal{O}} = (1/N_m) \sum_{i=1}^{N_m} \mathcal{O}_i$ of an observable $\mathcal{O} = \langle \overline{\mathcal{O}} \rangle$ measured in an importance sampling Monte Carlo process is given, in general, by the error estimate

$$\Delta \overline{\mathcal{O}} = \sqrt{\frac{\sigma_{\mathcal{O}_i}^2}{N_m}} \sqrt{2\tau_{\text{int}}}, \quad (1)$$

where $\sigma_{\mathcal{O}_i}^2$ is the variance of the individual autocorrelated measurements \mathcal{O}_i at “time” i , τ_{int} is the integrated autocorrelation time, and N_m is the total number of measurements. As it appears, there are three ways to reduce the statistical error. The most obvious but most expensive one is to increase the number of measurements. Since, however, $1/\sqrt{N_m}$ is a rather slowly decreasing function and, in the physically interesting continuum limit, it may happen that both the variance and the autocorrelation time diverge with some power of the discretization parameter, it is much more promising

to ask whether the statistical error may also be reduced by constructing an estimator for \mathcal{O} with a smaller variance or by employing refined update algorithms with smaller autocorrelation times. As we shall see below, the latter two strategies are to some extent intertwined, a fact which calls for a careful analysis.

In this paper we will focus on energy estimation. It is well known that in path-integral Monte Carlo simulations the energy may be measured using two different estimators. One is derived by a straightforward differentiation of the partition function and will be called for the sake of brevity the “kinetic” estimator since it involves an explicit measurement of the kinetic part of the energy.² The other is based on the virial theorem for path integrals and will hence be referred to as the “virial” estimator.^{3,4} The “virial” estimator is often judged to be the “better” estimator because in the continuum limit its variance is much smaller than that of the “kinetic” estimator.

Early investigations of the “kinetic” and the “virial” estimators focussed on their variances.^{4,5} In the following years it was pointed out that a correct assessment of the accuracy also has to take into account the autocorrelations, and it was demonstrated that for a standard Metropolis simulation of the harmonic oscillator the allegedly less successful “kinetic” estimator gave smaller errors than the “virial” estimator.⁶ In a further investigation⁷ it was shown that conclusions about the accuracy also depend on the particular Monte Carlo update algorithm at hand since modifications of the update scheme such as inclusion of collective moves of the whole path affect the autocorrelations of the two estimators in a different way.

For a fair judgement of the performance of an estimator, one thus has to take into account both the variances and the associated autocorrelation times. In this paper we analyze this problem for the two standard estimators in combination with four different update algorithms, namely (1) the standard Metropolis algorithm, (2) the multigrid V-cycle, (3) the multigrid W-cycle, and (4) the staging algorithm. The Metropolis algorithm is based on *local* moves and exhibits severe slowing down in the continuum limit.^{8,9} The other three update algorithms employ *non-local* moves and therefore reduce (V-cycle) or even completely overcome (W-cycle, staging) the slowing-down problem.^{9,10} As our main result we will then demonstrate how the estimation of energy can be improved at practically no extra cost by taking a suitable linear combination of the two estimators. We shall see that the optimal combination has to take into account not only the variances of the two individual

estimators but also their covariance, i.e., the cross-correlations between the two estimators.

The outline of the paper is as follows. In the next section we first recall the definition of the kinetic and virial estimators for the energy and discuss some of their basic properties. We then introduce the “combined” estimator and present a theoretical analysis of its properties. In Sec. 3 we define autocorrelation times and describe how our error analysis was performed. The various update algorithms are briefly summarized in Sec. 4. The results of the numerical simulations are contained in Sec. 5, and in Sec. 6 we close with our conclusions and a few final remarks.

2 Energy estimators

For didactic reasons we shall illustrate the improved energy estimation for simple one-particle quantum systems governed by a Hamiltonian¹¹

$$\hat{H} = \frac{1}{2m}\hat{p}^2 + V(\hat{x}). \quad (2)$$

where m is the mass of the particle and $V(x)$ a potential to be specified below. Our theoretical considerations are, however, completely general and without any additional problems applicable to many-body quantum systems as well. When coupled to a heat-bath at inverse temperature $\beta = 1/k_B T$, the canonical partition function is given in the operator representation by

$$\mathcal{Z}(\beta) = \text{Tr} e^{-\beta \hat{H}} = \sum_n e^{-\beta E_n}, \quad (3)$$

where E_n are the energy eigenvalues associated with (2). The equivalent path-integral representation¹² we wish to simulate reads ($\hbar \equiv 1$)

$$\mathcal{Z}(\beta) = \int \mathcal{D}x \exp \left\{ - \int_0^\beta d\tau \left[\frac{m}{2} \dot{x}^2 + V(x(\tau)) \right] \right\} = \lim_{L \rightarrow \infty} \mathcal{Z}^{(L)}(\beta), \quad (4)$$

where $\mathcal{Z}^{(L)}$ is the discretized path integral,

$$\mathcal{Z}^{(L)}(\beta) = \left[\prod_{k=1}^L \int_{-\infty}^{\infty} \frac{dx_k}{\sqrt{2\pi\epsilon/m}} \right] \exp \left\{ - \sum_{k=1}^L \left[\frac{m}{2\epsilon} (x_k - x_{k-1})^2 + \epsilon V(x_k) \right] \right\}, \quad (5)$$

with $\epsilon = \beta/L$ being the usual discretization parameter. The trace in (3) implies periodic boundary conditions, i.e., in (5) we take $x_0 = x_L$.

For the potential $V(x)$ we chose two characteristic shapes covering a wide range of physical phenomena. The first one is an anharmonic convex potential,

$$V(x) = 0.5x^2 + x^4 \quad (\text{CP}), \quad (6)$$

relevant for studying fluctuations around a unique minimum, and the second one is a double-well potential,

$$V(x) = -0.5x^2 + 0.04x^4 \quad (\text{DW}), \quad (7)$$

which exhibits tunneling phenomena.

2.1 The “kinetic” estimator

From the partition function (3) it is clear that the average energy is defined by

$$U = \langle \hat{H} \rangle = -\frac{\partial \ln \mathcal{Z}}{\partial \beta} = \text{Tr} \hat{H} e^{-\beta \hat{H}} / \mathcal{Z} = \frac{\sum_n E_n e^{-\beta E_n}}{\sum_n e^{-\beta E_n}}. \quad (8)$$

Since $\partial/\partial\beta = (1/L)\partial/\partial\epsilon$ it is easy to see that we get, in the path-integral representation, $U = \lim_{L \rightarrow \infty} U^{(L)}$ with $U^{(L)} = \langle U_k \rangle$ and

$$U_k = \frac{L}{2\beta} - \frac{m}{2L} \sum_{k=1}^L \left(\frac{x_k - x_{k-1}}{\epsilon} \right)^2 + \frac{1}{L} \sum_{k=1}^L V(x_k), \quad (9)$$

and $\langle \dots \rangle$ now means expectation values with respect to the discretized path integral (5), which are therefore also L -dependent. The term $L/2\beta$ stems from the β -dependence of the measure. For the sake of brevity we will in the sequel refer to the energy estimator (9) as the *kinetic* estimator² of the energy identified by a subscript k since it involves an explicit measurement of $\langle p^2/2m \rangle = \lim_{L \rightarrow \infty} \langle T_k \rangle^{(L)}$, with

$$T_k \equiv \frac{L}{2\beta} - \frac{m}{2L} \sum_{k=1}^L \left(\frac{x_k - x_{k-1}}{\epsilon} \right)^2 \quad (10)$$

being the path-integral estimator of the kinetic part of the energy. Notice that the kinetic part is *not* given by

$$\frac{m}{2} \langle v_k^2 \rangle \equiv \frac{m}{2} \left\langle \frac{1}{L} \sum_{k=1}^L \left(\frac{x_k - x_{k-1}}{\epsilon} \right)^2 \right\rangle, \quad (11)$$

as one might have naively guessed, since for all reasonably well behaved potentials $m\langle v_k^2 \rangle/2 = L/2\beta + \mathcal{O}(1)$ diverges as $L \rightarrow \infty$ (and β fixed as usual). For the proper definition, however, this piece is just needed to cancel the divergence coming from the measure.

Numerically it appears questionable, however, at first sight whether this estimator is very useful. The reason is that most of the signal of $\langle (x_k - x_{k-1})^2 \rangle$ is used to cancel the explicit $L/2\beta$ term. We would therefore expect that the variance of the “kinetic” estimator,

$$\sigma_k^2 = \langle U_k^2 \rangle - \langle U_k \rangle^2, \quad (12)$$

diverges linearly with L , and we would hence expect large statistical errors in the continuum limit of the path integral even for update algorithms which overcome the slowing down problem mentioned in the Introduction. This is what we indeed observed empirically; see the discussion in section 5 below. What we need is another estimator \tilde{T} for the kinetic energy with the *same mean*, $\langle \tilde{T} \rangle = \langle \hat{p}^2/2m \rangle$, but *smaller variance*. In the statistical literature this would run under the label of a “variance reduced” estimator. One possible candidate is suggested by means of the path-integral version of the *virial theorem*.

2.2 The “virial” estimator

In operator language the virial theorem states that¹⁴

$$\langle \frac{\hat{p}^2}{2m} \rangle = \frac{1}{2} \langle \hat{x} V'(\hat{x}) \rangle \quad (13)$$

where we have used the abbreviation $V'(x) = dV/dx$. From the above discussion one may guess that the path-integral analog should read

$$\frac{L}{2\beta} - \frac{m}{2} \langle \left(\frac{x_k - x_{k-1}}{\epsilon} \right)^2 \rangle = \frac{1}{2} \langle x_k V'(x_k) \rangle. \quad (14)$$

This relation indeed follows from the invariance of the partition function under a rescaling of the “field” x_k . To show this, we start from eq. (5) and rescale the “field” $x_k \rightarrow \lambda x_k$, which gives

$$\mathcal{Z}^{(L)} = \left[\prod_{i=1}^L \int_{-\infty}^{\infty} \frac{dx_k}{\sqrt{\frac{2\pi\epsilon}{m\lambda^2}}} \right] \exp \left\{ - \sum_{i=1}^L \left[\frac{m}{2\epsilon} \lambda^2 (x_k - x_{k-1})^2 + \epsilon V(\lambda x_k) \right] \right\}. \quad (15)$$

By choosing $\lambda^2 \equiv \epsilon/m$ the factor in front of the kinetic term becomes 1/2 and also the β -dependence of the measure vanishes. Differentiation with respect to β now only affects the potential energy term. Noting that $\partial V(\lambda x)/\partial \lambda = x \partial V(y)/\partial y|_{y=\lambda x}$, and rescaling variables back after differentiation, one readily arrives at $U^{(L)} = \langle U_v \rangle$ with the alternative “virial” estimator^{3,4}

$$U_v = \frac{1}{2L} \sum_{k=1}^L x_k V'(x_k) + \frac{1}{L} \sum_{k=1}^L V(x_k). \quad (16)$$

From here we deduce the virial theorem (14) with the well-behaved kinetic energy estimator $T_v = \frac{1}{2L} \sum_{k=1}^L x_k V'(x_k)$. The subscript v is a reminder of the fact that this energy estimator was derived using the virial theorem or, alternatively, that, in contrast to the “kinetic” estimator, it only refers to the potential $V(x_k)$. An alternative derivation of this estimator which makes use of the very same rescaling invariance would again start by rescaling the “field” x_k in the partition function (5) by $x_k \rightarrow \lambda x_k$. Differentiating $\ln \mathcal{Z}^{(L)}$ with respect to λ and putting $\lambda = 1$, one obtains in fact directly relation (14). The virial estimator can also be derived in yet another way.⁴

Notice that using the (incorrect) estimator $\frac{m}{2} \langle v_k^2 \rangle$, identifying it (incorrectly) with $\langle \frac{\hat{p}^2}{2m} \rangle$, applying the (correct) identity (operator formulation of the virial theorem), $\langle \frac{\hat{p}^2}{2m} \rangle = \langle \frac{1}{2} \hat{x} V'(\hat{x}) \rangle$, and identifying $\langle \frac{1}{2} \hat{x} V'(\hat{x}) \rangle$ (correctly) with $\langle \frac{1}{2} x_k V'(x_k) \rangle$ one arrives (accidentally) at the same result, but the derivation is clearly dubious.

2.3 Discussion of the two estimators

As explained above, the variance of the measured energies is a property of the estimators we employ. Regarding the dependence on the discretization, we expect asymptotically for large L a linear divergence of the variance for the “kinetic” estimator whereas the variance should stay roughly constant for the “virial” estimator. We emphasize that this dependence is completely independent of the update algorithm.

For purposes of illustration we show in Fig. 1 the variance of the two estimators as a function of the number of variables L . Since the update algorithm only affects the autocorrelation times and is *a priori* irrelevant for the variance of the individual measurements we may choose data for any update algorithm. In Fig. 1 we have used the data obtained by the multigrid

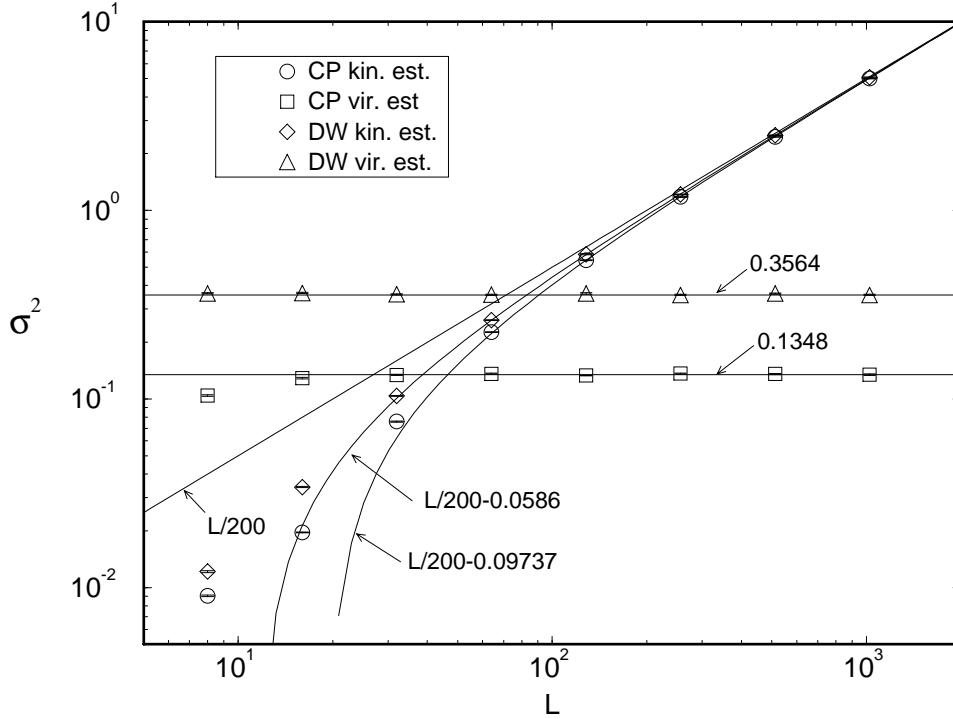


Figure 1: Variance of the individual energy measurements using the “kinetic” and the “virial” estimators for the two potentials (6) and (7) at $\beta = 10$. While the variance of the virial estimator is roughly constant in the continuum limit $L \rightarrow \infty$, the variance of the kinetic estimator asymptotically diverges as $\sigma_k^2 = L/2\beta^2$.

W-cycle, cf. the discussion in sections 4.2 and 5.1 and Table 3 below. As expected, the measured variances for the virial estimator are indeed roughly constant for all values of L . Minor deviations from the asymptotic value of $\sigma_v^2 = 0.1348(12)$ (CP) resp. $0.3564(24)$ (DW) (cp. Table 3) are observed only for the coarsest discretization of $L = 8$.

The behaviour is clearly different for the kinetic energy estimator. We first observe that for both potentials the divergence turns indeed out to be linear for large enough values of L . The straight line in Fig. 1 is the expected asymptotic behaviour of $\sigma_k^2 \rightarrow L/2\beta^2$, which in fact fits the data well for $L = 256, 512$, and 1024 . In order to account for the discrepancies which are observed for smaller values of L , we looked at the first correction term for σ_k^2 . A straightforward calculation shows that the variance (12) of the kinetic

estimator is given quite generally by

$$\sigma_k^2 = \frac{L}{2\beta^2} + \frac{C}{\beta^2} - \frac{1}{\beta} \langle x_i V'(x_i) \rangle, \quad (17)$$

where $C = -\beta^2 \partial U / \partial \beta$ is the specific heat. Instead of evaluating C directly we first calculate the variance of the virial estimator,

$$\sigma_v^2 = \frac{C}{\beta^2} + \frac{1}{\beta} \langle \frac{3}{4} x_i V'(x_i) + \frac{1}{4} x_i^2 V''(x_i) \rangle \quad (18)$$

which allows us to express σ_k^2 as

$$\sigma_k^2 = \frac{L}{2\beta^2} + \sigma_v^2 - \frac{1}{\beta} \langle \frac{7}{4} x_i V'(x_i) + \frac{1}{4} x_i^2 V''(x_i) \rangle. \quad (19)$$

For the quartic potential $V(x) = \omega^2 x^2/2 + gx^4$ we then find

$$\langle \frac{7}{4} x_i V'(x_i) + \frac{1}{4} x_i^2 V''(x_i) \rangle = 2\omega^2 \langle x_i^2 \rangle + 10g \langle x_i^4 \rangle. \quad (20)$$

The expectation value on the right hand side can be expanded as $a_0 + a_1/L^2 + a_2/L^4 + \dots$. In order to compute the first correction term a_0 we now use expectation values for the moments for $L = 128$, assuming that the $1/L^2$ corrections are already negligible for this value of L . At $\beta = 10$ we obtained (in a separate simulation using the staging algorithm) $\langle x_i^2 \rangle = 0.25660(46)$ and $\langle x_i^4 \rangle = 0.18085(62)$ for the convex potential (CP, $\omega^2 = 1$, $g = 1$), resp. $5.391(18)$ and $37.33(19)$ for the double-well potential (DW, $\omega^2 = -1$, $g = 0.04$). Numerically, we therefore find the correction terms to be $a_0 = 2.3217$ (CP) resp. 4.1500 (DW), and together with the asymptotic values of $\sigma_v^2 = 0.1348$ (CP) resp. 0.3564 (DW) we finally arrive at $\sigma_k^2 - L/2\beta^2 = -0.09737$ (CP) resp. -0.0586 (DW). As can be seen from Fig. 1, taking into account this first correction does indeed reproduce the data down to at least $L = 64$. Clearly, for smaller values of L we would need to evaluate the higher-order coefficients a_1 , a_2 , etc., in order to reproduce the values for σ_k^2 .

In summary, we have illustrated the expected behaviour that the variances of the measurements are roughly independent from L for the virial estimator but diverge linearly for large values of L for the kinetic estimator. Before going on we finally remark that the two different energy estimators also entail two different estimators for the specific heat by virtue of the relation

$$\langle C_{k,v} \rangle = -\beta^2 \frac{\partial \langle U_{k,v} \rangle}{\partial \beta}. \quad (21)$$

2.4 The “combined” estimator

In the Monte Carlo process we are measuring the energy using either the “kinetic” estimator (9) or the “virial” estimator (16) for the configurations $\{x_j\}_i$. This procedure yields the two mean values $\bar{U}_k \equiv \sum_{i=1}^{N_m} U_{k,i}/N_m$ and $\bar{U}_v \equiv \sum_{i=1}^{N_m} U_{v,i}/N_m$ as stochastic variables with the same expectation value, $\langle \bar{U}_k \rangle = \langle \bar{U}_v \rangle = U$, but different statistical errors. Let us here abbreviate the *variances of the mean values* (i.e., the squared errors) by $\Delta_k^2 \equiv (\Delta \bar{U}_k)^2 = \langle \bar{U}_k^2 \rangle - \langle \bar{U}_k \rangle^2$ and $\Delta_v^2 \equiv (\Delta \bar{U}_v)^2 = \langle \bar{U}_v^2 \rangle - \langle \bar{U}_v \rangle^2$.

It is clear that any linear combination of the form

$$\bar{U}_c(\alpha) = \alpha \bar{U}_k + (1 - \alpha) \bar{U}_v \quad (22)$$

would also give the same expectation value, $\langle \bar{U}_c \rangle = U$, as the individual estimators alone. The variance $\Delta_c^2 \equiv (\Delta \bar{U}_c)^2$ of the combined estimator \bar{U}_c would be given by

$$\begin{aligned} \Delta_c^2 &= \langle (\alpha \bar{U}_k + (1 - \alpha) \bar{U}_v)^2 \rangle - \langle \alpha \bar{U}_k + (1 - \alpha) \bar{U}_v \rangle^2 \\ &= \alpha^2 \Delta_k^2 + 2\alpha(1 - \alpha) \Delta_{kv}^2 + (1 - \alpha)^2 \Delta_v^2, \end{aligned} \quad (23)$$

where $\Delta_{kv}^2 = \langle \bar{U}_k \bar{U}_v \rangle - \langle \bar{U}_k \rangle \langle \bar{U}_v \rangle$ is the covariance of the mean values of the two estimators. Minimizing the variance Δ_c^2 with respect to the parameter α yields the optimal α as

$$\alpha_{\text{opt}} = \frac{\Delta_v^2 - \Delta_{kv}^2}{\Delta_k^2 + \Delta_v^2 - 2\Delta_{kv}^2}. \quad (24)$$

Inserting this optimal α_{opt} into eq. (23) one obtains an expression for the minimal variance of $\bar{U}_c(\alpha)$ which reads

$$\begin{aligned} \Delta_{c,\text{opt}}^2 &= \frac{\Delta_k^2 \Delta_v^2 - (\Delta_{kv}^2)^2}{\Delta_k^2 + \Delta_v^2 - 2\Delta_{kv}^2} \\ &= \frac{1 - \rho^2}{1/\Delta_k^2 + 1/\Delta_v^2 - 2\rho/\Delta_k \Delta_v}, \end{aligned} \quad (25)$$

where $\rho = \Delta_{kv}^2/(\Delta_k \Delta_v)$ is the correlation coefficient of \bar{U}_k and \bar{U}_v . If the two estimators were completely decorrelated, $\rho = 0$, the optimal combination of the two estimators would simply be the error weighted mean of the individual

estimators. If the variances Δ_k^2 and Δ_v^2 furthermore were equal, the error Δ_c would be reduced by a factor of $\sqrt{2}$, i.e., one would effectively gain a factor of 2 in the run time. If on the other hand the two variances were very much different we would not gain very much, since the less accurate estimator would hardly get any weight in (22) (i.e., $\alpha \approx 0$ or $\alpha \approx 1$).

The optimal combination of the two estimators involves, however, the covariance of the two estimators and therefore is in general not simply given as the error weighted mean of the individual estimators. In fact, erroneously ignoring the covariance of the two estimators might lead to the irritating result that the variance of the combined estimator is not even reduced with respect to the smaller one of the two individual estimators.

As it turns out, taking properly into account the covariance of the two estimators it may even happen that $\alpha > 1$ or $\alpha < 0$, and it may also happen that the error of the combined estimator is even *more* reduced than by the factor of $\sqrt{2}$, which might naively be expected to be an upper bound for the gain in accuracy.

For further discussion, let us assume without loss of generality that $\Delta_v \leq \Delta_k$ and let us introduce the ratio $\kappa = \Delta_v/\Delta_k \leq 1$. The optimal parameter α_{opt} may then be expressed as

$$\alpha_{\text{opt}} = \frac{\kappa^2 - \rho\kappa}{1 + \kappa^2 - 2\rho\kappa}, \quad (26)$$

and the reduction of the error may be judged by looking at the quantity

$$R \equiv \frac{\Delta_{c,\text{opt}}^2}{\Delta_v^2} = \frac{1 - \rho^2}{1 + \kappa^2 - 2\rho\kappa}, \quad (27)$$

which by definition satisfies $0 \leq R \leq 1$. The smaller R , the greater the gain by using the combined estimator. For an overview of possible situations, we plot α_{opt} and R as a function of the ratio κ and the correlation coefficient ρ in Figs. 2 and 3.

In Fig. 2 we first notice that for vanishing covariance, $\rho = 0$, the optimal interpolation parameter α_{opt} is always in the range $0 \leq \alpha_{\text{opt}} \leq 1$. For completely correlated data, $\rho = 1$, on the other hand, the optimal interpolation parameter is always negative, $\alpha_{\text{opt}} = \kappa/(\kappa - 1) < 0$.

Taking a look at the error reduction factor R in Fig. 3 we notice again, that for completely decorrelated data $\rho = 0$, nothing spectacular happens.

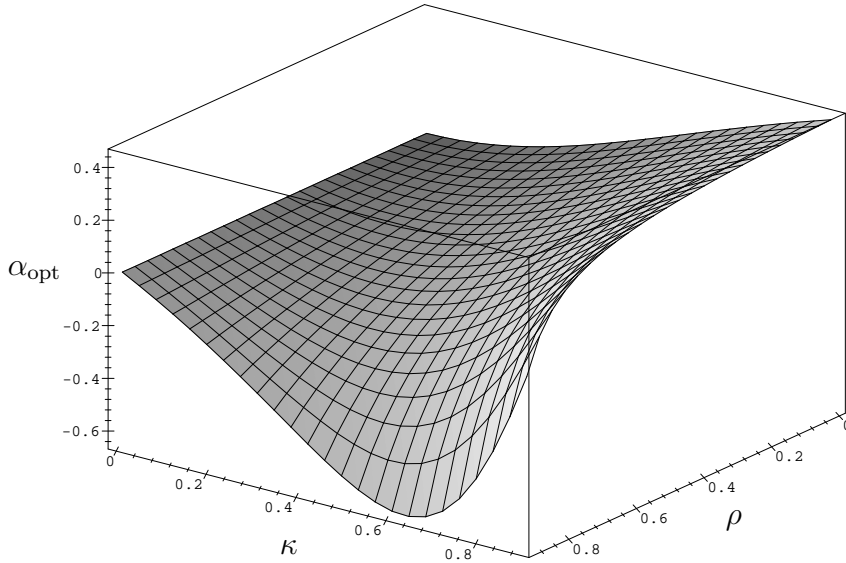


Figure 2: The optimal interpolation parameter α_{opt} as given in eq. (26) as a function of the ratio $\kappa = \Delta_v/\Delta_k$ and the correlation coefficient $\rho = \Delta_{kv}^2/(\Delta_k\Delta_v)$.

The gain is best if the variances of the two estimators are equal, $\kappa = 1$, and there is no gain at all, if the smaller variance is negligible compared to the larger one, $\kappa = 0$. The situation is very different though for highly correlated data, $\rho \rightarrow 1$. We first observe that in this case the gain can be much more profitable than the best gain of $R = 0.5$ for completely decorrelated data. Assuming, for example, a correlation of $\rho = 0.9$ and a ratio of $\kappa = 0.5$ we find that the reduction factor is $R \approx 0.21$, i.e. the variance of the combined estimator is then roughly 5 times smaller than the smaller of the individual variances. It should be noted that for cross-correlated data there is in fact no limit to the gain in efficiency, and that, as a general rule, the gain is largest for two estimators which are highly correlated and have very different variances. Notice that for $\rho \approx 0$ the inverse gain factor R is a decreasing function of κ (highest gain for comparable variances), while for $\rho \approx 1$ the situation is just reversed, i.e., R increases with κ (highest gain for very different variances).

In order to illustrate the combination of the two estimators with actual

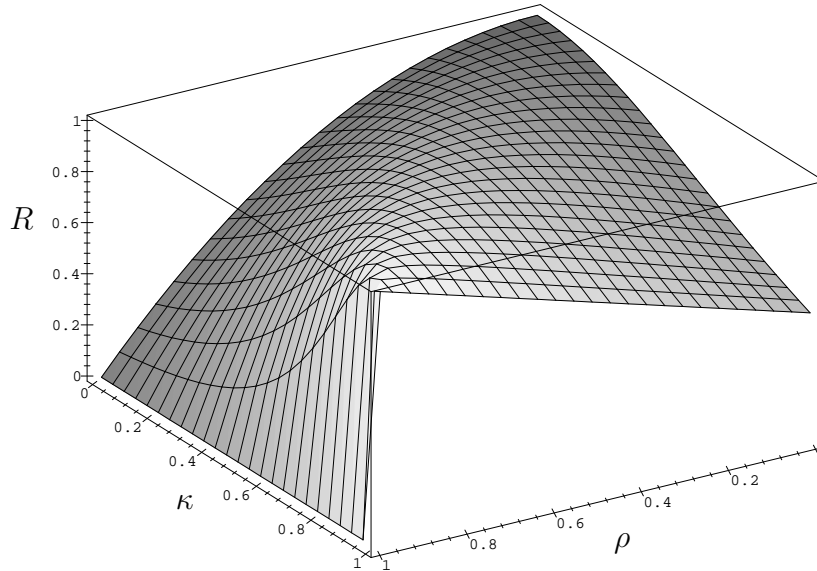


Figure 3: The reduction factor R as given in eq. (27) as a function of the ratio $\kappa = \Delta_v/\Delta_k$ and the correlation coefficient $\rho = \Delta_{kv}^2/(\Delta_k\Delta_v)$.

simulation data (using data for the convex potential obtained by multigrid W-cycle updating), we show in Fig. 4 the relative statistical error as a function of the interpolation parameter α . In order to simulate the measurement of an arbitrary combination of the two estimators, the data points in Fig. 4 were obtained from a time series of an estimator $U_c(\alpha)$ for arbitrary α which was generated from the time series of each of the individual measurements of U_k and U_v . The time series for $U_c(\alpha)$ was then subsequently analysed for each α by the usual jackknife blocking procedure to obtain the error estimate (cf. section 3.2). The solid lines interpolating these data points, on the other hand, were computed using eq. (23) with the variances and covariance of U_k and U_v obtained by the jackknife method on the basis of 100 blocks.

We see that the theoretically expected error (23) reproduces indeed the empirically measured errors for a linear combination of the two estimators at each measurement. We emphasize that the combination can hence always be done post simulation without any restriction, as long as the variances *and* the covariance of the two estimators have been measured (i.e., it is *not* necessary to store the complete time series of U_k and U_v which, in some applications,

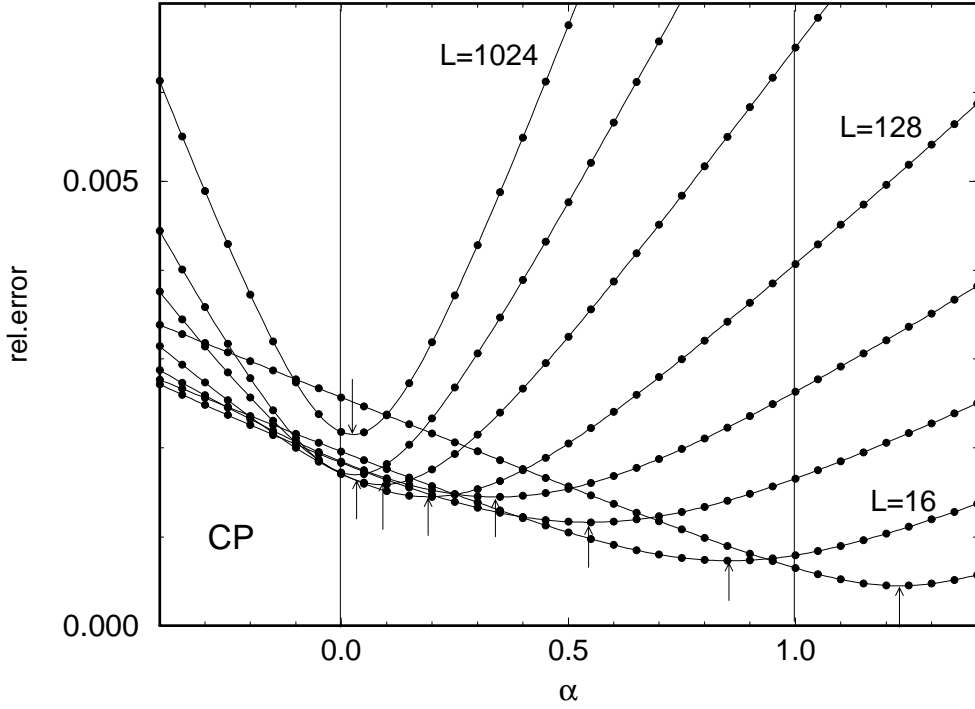


Figure 4: Relative statistical error $\Delta\bar{U}_c/\bar{U}_c$ of the linear combination \bar{U}_c of the two energy estimators for the convex potential as a function of the interpolation parameter α (using the W-cycle update algorithm). Data symbols denote jackknife averages over 100 blocks, and the solid lines are computed according to the theoretical prediction (23), using as input only the (jackknife) variances of the virial and the kinetic estimator (corresponding to $\alpha = 0$, resp. $\alpha = 1$) and the (jackknife) covariance of the two estimators. The arrows indicate the values of optimal α according to eq. (24).

might cause disk-space problems).

The arrows indicate the locations of the optimal values of α computed according to eq. (24). These values are also reported in Table 1 together with the correlation coefficient ρ and the measured energies using the optimal combination. We note that for the coarsest discretization of $L = 8$ we do indeed find a case where the optimal interpolation parameter α falls outside the usually expected range of $[0, 1]$. Unfortunately, in this application the theoretically possible error reduction for correlated estimators is not realized, and the physically interesting data are those for large L , where the correlation coefficient is only about $\rho = 0.3 - 0.5$. Very similar plots were obtained for the case of the double-well potential.

At this point it should be stressed that, in general, the question of how much the error can be reduced in the simulation of a particular problem at hand appears to be an empirical question. As a general lesson, we emphasize that the fact that two independent estimators are correlated does not necessarily mean bad news. The gain in efficiency crucially depends on both the correlation and the ratio of the individual variances. A further discussion will be given below in section 5.4.

3 Errors in the Monte Carlo process

In this paper we investigate both the variances and the autocorrelation times associated with different energy estimators. While the variance is a property of the partition function and the estimator alone, the autocorrelation time also depends on the update scheme and represents the relevant quantitative measure for the dynamics of the Monte Carlo process.

In general, the autocorrelation time τ is proportional to some power of the correlation length ξ of the system, $\tau \propto \xi^z$, with a dynamical critical exponent z . For standard local update algorithms the exponent z is close to 2 as can be argued in a simple random walk picture. For spin systems or field theoretic models undergoing a second-order phase transition the correlation length diverges and as soon as ξ exceeds the linear size L of the lattice the autocorrelation times diverge like $\tau \propto L^z$. In statistical mechanics and lattice field theory this problem is known under the name of *critical slowing down*.

In path-integral simulations a very similar problem occurs in the continuum limit $\epsilon \rightarrow 0$ with β fixed, or, equivalently, $L \rightarrow \infty$. The reason for this slowing down is easily understood. The correlations $\langle x_k x_{k+l} \rangle$ only depend on β and on the gaps between the energy levels. Hence the correlation length ξ only depends on the physical parameters at hand, and consequently always diverges linearly with L if measured in units of the lattice spacing ϵ . Thus we expect that the autocorrelation time for path-integral simulations grows as

$$\tau \propto L^z, \tag{28}$$

with a dynamical critical exponent z as well, and that for standard local algorithms $z = 2$. Note that in contrast to the infinite-volume limit in statistical mechanics, for path integrals also the Hamiltonian, i.e., the exponent in (5) changes its form in the limit $L \rightarrow \infty$ which is a characteristic feature

of path-integral simulations. As a consequence slowing down occurs in the continuum limit for *any* fixed β and *any* set of potential parameters.

3.1 Definition and measurement of autocorrelation times

Since the measurement of autocorrelation times will be of central concern in the remainder of this paper let us briefly recall the basic definitions.^{17,18}

In general, if \mathcal{O}_i denotes the i th measurement of an observable \mathcal{O} in the Monte Carlo process the (normalized) autocorrelation function $A(j)$ is defined by

$$A(j) = \frac{\langle \mathcal{O}_i \mathcal{O}_{i+j} \rangle - \langle \mathcal{O}_i \rangle^2}{\langle \mathcal{O}_i^2 \rangle - \langle \mathcal{O}_i \rangle^2}. \quad (29)$$

In Monte Carlo simulations we are always dealing with a *finite* number of measurements N_m . Nevertheless, computing the variance for the mean $\overline{\mathcal{O}}$ of measurements is straightforward and yields an error estimate of the form $\Delta \overline{\mathcal{O}} = \sqrt{2\tau_{\text{int}}(N_m)} \sqrt{\sigma^2/N_m}$, where N_m is the number of measurements used to compute the mean value $\overline{\mathcal{O}}$. Here $\tau_{\text{int}}(k)$ is an integrated autocorrelation time given by¹⁹

$$\tau_{\text{int}}(k) = \frac{1}{2} + \sum_{j=1}^k A(j) \left[1 - \frac{j}{N_m} \right]. \quad (30)$$

The effective statistics is thus reduced to $N_{\text{eff}} = N_m/2\tau_{\text{int}}(N_m)$. Or, in other words, to achieve a given error $\Delta \overline{\mathcal{O}}$ the run-time (i.e. the budget) has to be increased by a factor of $2\tau_{\text{int}}(N_m)$.

For large j the autocorrelation function $A(j)$ usually decays like an exponential

$$A(j) \xrightarrow{j \rightarrow \infty} a \exp(-j/\tau_{\text{exp}}), \quad (31)$$

where τ_{exp} denotes the exponential autocorrelation time and a is some constant. Since, in general, all these quantities depend on the observable under consideration we will indicate the relevant observable by an additional subscript unless it is clear from the context which observable is meant.

Due to the usual exponential decay of the autocorrelation function $A(j)$ and the large number of measurements N_m in a Monte Carlo simulation, the factor $\left[1 - \frac{j}{N_m} \right]$ in (30) accounting for the finite size of the statistical sample may in practical applications safely be neglected. In practice, one therefore usually computes the autocorrelation time by computing the sum in eq. (30)

without the correction factor and by cutting it off self-consistently at some k_{\max} such that $n_{\text{cut}}\tau_{\text{int}}(k_{\max}) \approx k_{\max} \ll N_m$. Usually n_{cut} is set equal to $n_{\text{cut}} = 6$ or 8 . As long as integrated and exponential autocorrelation times are roughly the same this method gives reliable estimates for τ_{int} . If exponential and integrated autocorrelation times are very much different from each other this method tends to underestimate the integrated autocorrelation time. This typically happens when the faster decaying modes neglected in (31) are still important for relatively large time lags j .

A more reliable way of determining the autocorrelation times in this case is to rewrite the integrated autocorrelation time as²⁰

$$\tau_{\text{int}}(k) = \tau_{\text{int}} - a \sum_{j=k+1}^{\infty} \exp(-j/\tau_{\text{exp}}) \quad (32)$$

$$= \tau_{\text{int}} - a \frac{\exp\{-1/\tau_{\text{exp}}\}}{1 - \exp\{-1/\tau_{\text{exp}}\}} \exp\{-k/\tau_{\text{exp}}\}, \quad (33)$$

where $\tau_{\text{int}} \equiv \tau_{\text{int}}(\infty)$. A three-parameter fit of $\tau_{\text{int}}(k)$ then gives both the integrated and the exponential autocorrelation times τ_{int} and τ_{exp} simultaneously, which is a further advantage of this method.

In Fig. 5 the behaviour of $A(j)$ and $\tau_{\text{int}}(k)$ of the virial estimator is illustrated for one typical example (CP potential, V-cycle multigrid update, $\beta = 10$, $L = 512$). A two-parameter fit of the autocorrelation function $A(j)$ according to eq. (31) in the range $j = 5, \dots, 15$ for this case gave values of $a = 0.619(33)$ and $\tau_{\text{exp,v}} = 7.23(40)$. A three-parameter fit of the integrated autocorrelation time according to eq. (33) in the same range yielded values of $a = 0.614(42)$, $\tau_{\text{exp,v}} = 7.26(48)$, and $\tau_{\text{int,v}} = 4.98(15)$. A determination of the integrated autocorrelation time via a self-consistent cutoff at $8\tau_{\text{int,v}}$ on the other hand yielded a value of $\tau_{\text{int,v}} = 5.07(21)$ (cp. Table 3). Clearly all values are consistent within error bars.

3.2 Blocking and jackknife procedures

Another way of estimating the true error of the Monte Carlo simulation is to divide the N_m measurements into n_{bl} blocks of size $N_{\text{bl}} = N_m/n_{\text{bl}}$ and compute the averages for each block separately. The block averages are then again stochastic variables with the same mean but reduced autocorrelations. In fact, if the block length is appreciably larger than the integrated autocorrelation time for the observable under consideration ($20\tau_{\text{int}}$, say, would

clearly be sufficient) than the block averages are (almost) uncorrelated and we can estimate the error of the observable from the variance of the block averages, $\Delta\overline{\mathcal{O}} = \sqrt{\sigma_{\mathcal{O},\text{bl}}^2/n_{\text{bl}}}$. Since n_{bl} should be at least around 20 to allow for a statistically meaningful estimation of $\sigma_{\mathcal{O},\text{bl}}^2$, the number of measurements per block is always much smaller than the total number of measurements, $N_{\text{bl}} \ll N_m$. For observables that can be estimated only with so-called biased estimators this may result in severe systematic errors when N_{bl} becomes too small.

It is therefore gratifying that bias-reduced and thus more accurate estimates of the errors can be achieved by using so-called jackknife blocking techniques.²¹ The main difference is that here the block averages are taken over the whole run with only one block excluded. These jackknife block averages have consequently a much reduced variance $\sigma_{\mathcal{O},\text{j-bl}}^2$ and the error estimate now reads $\Delta\overline{\mathcal{O}} = \sqrt{(n_{\text{bl}} - 1)\sigma_{\mathcal{O},\text{j-bl}}^2/n_{\text{bl}}}$, where the factor $(n_{\text{bl}} - 1)$ corrects for the trivial correlations between different jackknife blocks (because each measurement enters in *all but one* jackknife block – this has nothing to do with autocorrelations). It should be stressed that for unbiased estimators, such as arithmetic mean values, the blocking and jackknife blocking method give identical results. The advantages of jackknife blocking only show up for biased estimators, such as those for the specific heat or autocorrelation functions.

Using the blocking or jackknife blocking error estimate the integrated autocorrelation time for an observable \mathcal{O} can then also be obtained by inverting the standard error formula as

$$\tau_{\text{int}} = \frac{(\Delta\overline{\mathcal{O}})^2 N_m}{2\sigma_{\mathcal{O}_i}^2}, \quad (34)$$

where $\Delta\overline{\mathcal{O}}$ is the error measured in the blocking analysis and $\sigma_{\mathcal{O}_i}^2$ is the variance of the single (unblocked) measurements. It should be stressed that this method of estimating the integrated autocorrelation time is only valid if the block length N_{bl} is several times larger than the true integrated autocorrelation time. Otherwise τ_{int} will be systematically underestimated. At the same time we want to have, of course, as many blocks as possible in order to reduce the statistical error on the error estimates. Since $n_{\text{bl}}N_{\text{bl}} = N_m$ is fixed for a given statistics, these are conflicting requirements. If the measurements are not too strongly correlated, a reasonable compromise is the

choice $n_{\text{bl}} \approx N_{\text{bl}} \approx \sqrt{N_m}$.

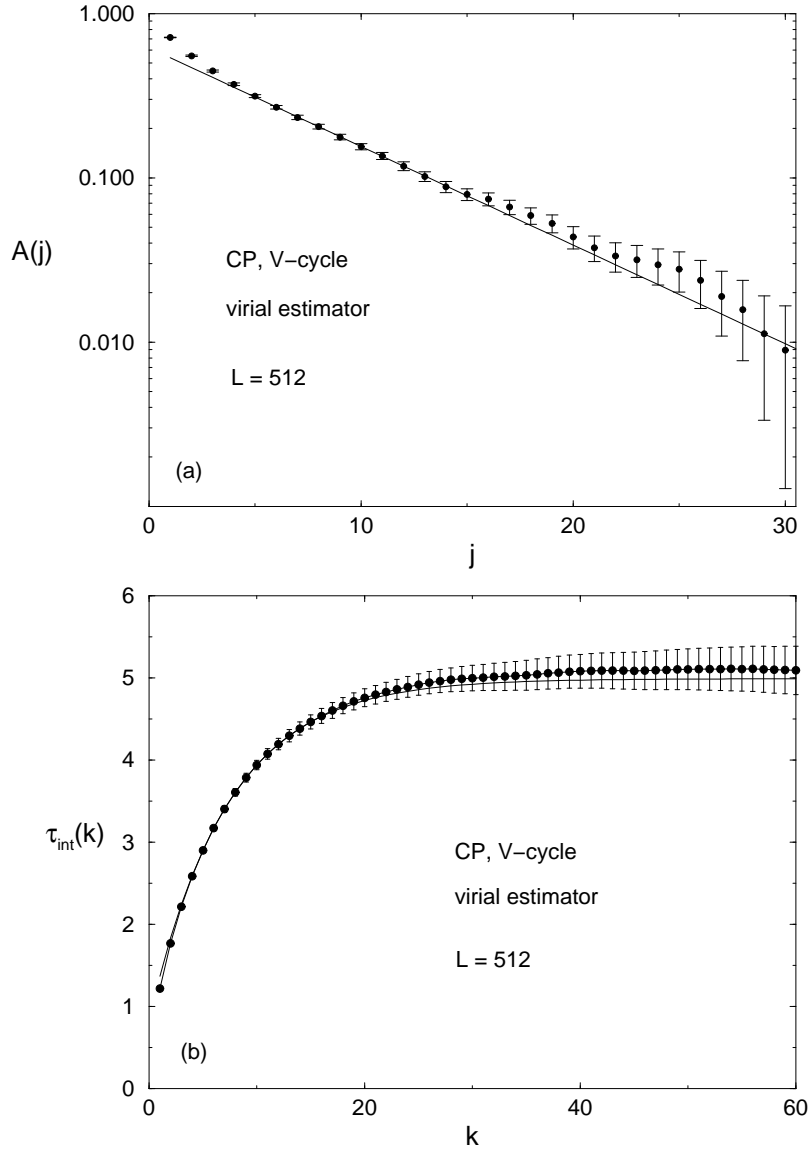


Figure 5: (a) The autocorrelation function $A(j)$ on a logarithmic scale and (b) the integrated autocorrelation time $\tau_{\text{int}}(k)$ of the virial estimator as obtained with the V-cycle multigrid algorithm for the convex potential (CP) at $\beta = 10$ and $L = 512$. Solid lines show fits according to eq. (31) resp. (33). The asymptotic value of $\tau_{\text{int}}(k)$ quoted in Table 3 is $\tau_{\text{int,v}} = 5.07(21)$.

4 Update algorithms

Before presenting our results in the next section, we will briefly review the update algorithms we have investigated, notably the multigrid method and the staging algorithm.

4.1 Local algorithms

The most extensively used algorithm for PIMC simulations still is the standard Metropolis algorithm.²² As far as accuracy and efficiency are concerned it has the well-known serious drawback of *local* algorithms that in the continuum limit $\epsilon = \beta/L \rightarrow 0$ the autocorrelation times diverge quadratically with the grid size, $\tau \propto L^2$, resulting in a severe slowing down of the Monte Carlo process, see the discussion in section 3. In spite of this drawback it is still widely used for its simplicity even though a lot of computer time might be saved by using more refined algorithms.

A local algorithm which does reduce slowing down to some extent is the hybrid overrelaxation method.²³ This algorithm mixes (deterministic) overrelaxed updates of the path with stochastic Metropolis sweeps. If the ratio of overrelaxed and Metropolis sweeps is chosen properly, i.e., in proportion to the spatial correlation length, this algorithm reduces slowing down to a linear divergence,^{8,24} $\tau \propto L$.

More successful are *non-local* algorithms which will be briefly described in the next two subsections.

4.2 Multigrid method

The basic idea of the multigrid approach^{25,26} is to perform non-local updates of the variables by working on a set of successively coarser discretizations of the time axis (“grids”) in order to take into account long wavelength fluctuations of the paths more efficiently. To this end one performs collective updates on different length scales by visiting various coarsened grids in a systematic order as extensively discussed in the context of partial differential equations.²⁶ The auxiliary variables on the coarsened grids are then interpolated back to the finer grids and eventually to the original grid using some specific interpolation scheme in a recursive manner. Equivalently, one may

also view the multigrid approach from a unigrid point of view where the update on a coarsened grid corresponds to a simultaneous move of a group of adjacent variables on the original grid. Using the so-called piecewise constant interpolation scheme for example, this amounts, in the unigrid viewpoint, to proposing moves for blocks of $1, 2^d, 4^d, \dots, V = L^d = 2^{nd}$ adjacent variables in conjunction. Here d is the dimension of the system under consideration. For PIMC simulations we usually have $d = 1$, even for quantum chains or quantum crystals since it may well suffice to use multigrid acceleration only along the Trotter direction of the discretized path integral.²⁷ Particular successful sequences of length scales 2^k are the so-called V-cycle with $k = 0, 1, \dots, n-1, n, n-1, \dots, 1, 0$, and the W-cycle whose graphical representation looks like the letter W (for $n = 3$, e.g., this is $k = 0, 1, 2, 3, 2, 3, 2, 1, 2, 3, 2, 3, 2, 1, 0$).²⁸ The update at level k thus consists in considering a common move Δx for all 2^{kd} variables of one block, $x_k \rightarrow x_k + \Delta x$, $i \in \text{block}$, computing the associated energy change and applying the usual accept/reject criterion.

The multigrid approach thus has a number of parameters which may be adjusted to suit the problem at hand, notably the choice of the interpolation scheme, the block length, the recursion scheme (e.g. V- or W-cycle), the number of updates on each grid in going down the recursion scheme (presweeps) and in going up again (postsweeps), and the Metropolis parameters for the coarsened grid updates. In the Gaussian case it is known that by using the piecewise constant interpolation scheme the V-cycle leads to a linear divergence of autocorrelation times, $\tau \propto L$, while the more successful W-cycle beats slowing down completely, $\tau \propto \text{const.}$ ⁹

Let us finally emphasize that the multigrid method can easily be applied to general d -dimensional lattice field theories. In fact, it is in this context where the stochastic multigrid Monte Carlo formulation appeared first in the literature,²⁵ and only quite recently these ideas have been adapted to path-integral simulations.^{8,9,29}

4.3 Staging algorithm

The basic idea of the staging algorithm³⁰ is to rewrite the discretized quantum statistical partition function (5) in such a way that a sequence of j adjacent variables can be updated one by one independently, i.e., by effectively removing the coupling between the variables. The coupling between

variables stems from the kinetic term and, in the continuum limit, $\epsilon \rightarrow 0$, the kinetic term $m/(2\epsilon)(x_k - x_{k-1})^2$ numerically starts to dominate over the potential energy term $\epsilon V(x_k)$. The kinetic term for adjacent variables can, however, trivially be rewritten as

$$(x_{k+1} - x_k)^2 + (x_{k+2} - x_{k+1})^2 = (x_{k+2} - x_k)^2/2 + 2(x_{k+1} - x_{k+1}^*)^2, \quad (35)$$

with $x_{k+1}^* \equiv (x_k + x_{k+2})/2$. The variable x_{k+1} can thus be decoupled from its neighbours. The crucial observation for the staging algorithm is that this can be iterated as

$$\frac{1}{j}(x_{k+j} - x_k)^2 + (x_{k+j+1} - x_{k+j})^2 = \frac{1}{(j+1)}(x_{k+j+1} - x_k)^2 + \frac{j+1}{j}(x_{k+j} - x_{k+j}^*)^2, \quad (36)$$

with new variables $x_{k+j}^* \equiv (x_k + x_{k+j+1})/(j+1)$. A sequence of free particle propagators can thus be rewritten as³⁰

$$\prod_{i=0}^j \langle x_{k+i} | \exp(-\epsilon \frac{1}{2m} \hat{p}^2) | x_{k+i+1} \rangle = \langle x_k | \exp(-j\epsilon \frac{1}{2m} \hat{p}^2) | x_{k+j+1} \rangle \prod_{i=2}^j \left[\frac{m_i}{2\pi\epsilon} \right]^{1/2} \exp\left(-\frac{m_i}{2\epsilon}(x_i - x_i^*)^2\right), \quad (37)$$

where renormalized masses $m_i \equiv \frac{i}{i-1}m$ have been introduced. Selecting the end points x_k and x_{k+j+1} of some segment of the discretized path with j “beads” in between, one can thus perform a (recursive) change of variables $x_{k+i} \rightarrow x_{k+i}^*$, $i = 1, \dots, j$, in the discretized partition function (5). For the staging segment, this would eliminate the nearest neighbour coupling stemming from the kinetic energy. For the variables of the staging segment the partition function hence reduces to a collection of independent oscillators moving in an external potential which depends on the transformation of the variables. The staging variables may then be updated using Gaussian random variables $u_k \equiv x_k - x_k^*$ with “masses” m_i , and a Metropolis like acceptance rule for the external potential.

In contrast to the multigrid method the staging algorithm only allows for one single tunable parameter, the length j of the staging segment. The optimal choice of the staging parameter j depends on the observable of interest, its estimator and on the discretization. But since it is the greater mobility of the variables of the staging segment which reduces autocorrelation times

the optimal staging length j_{opt} scales with the correlation length along the path, i.e., it scales with the number of variables L in the discretized partition function.¹⁰ For an appropriate choice of j_{opt} the staging algorithm then completely reduces slowing down in the continuum limit, $\tau \propto \text{const.}$ Thus, both the staging and multigrid W-cycle represent refined PIMC update schemes which beat the continuum slowing down. Elsewhere we have compared the two algorithm and discussed their mutual merit in more detail.¹⁰

5 Results

5.1 Simulation details

For each of the four update algorithms described above (Metropolis, multigrid V- and W-cycle, staging algorithm) we simulated the path integral (5) for grids of size $L = 2^3 = 8$ up to $L = 2^{10} = 1024$ sites. In all our simulations the mass m was set equal to 1 and the inverse temperature was equal to $\beta = 10$. In our simulations we performed $N_m = 100\,000$ updates of the path after discarding 5 000 initial updates of the path for thermalization.

In the case of the Metropolis algorithm an “update of the path” here means n_e sweeps over the full path with single-hit updates of each site with roughly 50% acceptance probability. In order to accurately assess autocorrelation times, the parameter n_e was adjusted in such a way that the autocorrelation times in units of measurements were comparable for all grid sizes L . For the convex potential this could always be achieved by setting $n_e = 1$, except for $L = 256, 512$, and 1024 where we had $n_e = 5, 20$, and 80 , respectively. For the double-well potential we started out with $n_e = 1, 1, 1$, and 2 for $L = 8, 16, 32$, and 64 . For the larger grid sizes, however, the autocorrelation times in units of single sweeps turned out to be so different for the two estimators that we actually performed two sets of simulations with different choices of n_e (the combined estimator then obviously makes no sense). In the first set, focusing on the autocorrelation time for the kinetic estimator, we could still use $n_e = 1$, except for the largest grid $L = 1024$ where we set $n_e = 6$. In these runs the autocorrelation times for the virial estimator turned out to be far too big to be measurable on the larger grids. To satisfy our own curiosity and to measure autocorrelation times for the virial estimator as well, we therefore performed a second set of simulations

with $n_e = 15, 60, 150$, and 600 for $L = 128, 256, 512$, and 1024 , respectively, even though this clearly requires employing CPU resources out of proportion. In the following, all autocorrelation times for the Metropolis algorithm will be given in units of single sweeps.

In the case of the multigrid algorithm an “update of the path” means a complete V- resp. W-cycle with $n_{\text{pre}} = 1$ presweeps and $n_{\text{post}} = 0$ postsweeps. On each grid we performed single-hit Metropolis updates with an acceptance rate of 40% – 60% which for the system at hand could be achieved with the same maximal step width on all grids.

In the case of the staging algorithm, an “update of the path” means $\text{int}(L/(j-1))$ calls to the staging routine which moves $j-1$ adjacent variables at each call. The choice of the staging length j is shown in Table 5 below. For the analysis of the combined estimator we used the same j as for the virial estimator. This will be discussed in more detail below in section 5.4. Notice that the above definition in general implies updates of less than L variables. We have therefore rescaled the actually measured autocorrelation times by a factor $(\text{int}(L/(j-1)))/(L/(j-1))$. This enables a direct comparison of the staging algorithm with the standard Metropolis algorithm. A comparison with the multigrid method has to take into account a constant factor for the V-cycle (which of course depends on the implementation but should theoretically be ≈ 2) and an extra factor of $\log L$ for the W-cycle.

After each update of the path we measured the internal energy using both the “kinetic” estimator (9) and the “virial” estimator (16). The time series of these measurements were then analysed by jackkniving the data on the basis of 100 blocks. Autocorrelation times were obtained by cutting $\tau_{\text{int}}(k)$ self-consistently at $k_{\text{max}} = 8$. The reported errors for the autocorrelation times were again obtained by jackkniving.

With these remarks in mind we emphasize that our data now allow for a precise and detailed comparison of the commonly used energy estimators taking into account the dynamics of different update schemes.

5.2 Results for the energy

Tables 1 and 2 show the measured energies for the convex potential (CP) and for the double-well potential (DW) using the “kinetic” estimator and the “virial” estimator as well as using the optimally combined estimator. For ease of comparison we also give for each energy measurement the rela-

tive error in percent. In addition, for the combined estimator, we list the correlation coefficient ρ and the parameter α_{opt} used for computing the combined estimator according to eq. (22).

Since in our simulations we saved the time series of the U_{k} - and U_{v} -measurements, we were able to compute a posteriori time series of U_{c} for any α which could then be analyzed in the same fashion as the (run-)time series for the “kinetic” and the “virial” estimator. The energy values and the jackknife errors reported in Tables 1 and 2 were thus obtained by analyzing the time series of the combined estimator $U_{\text{c}}(\alpha_{\text{opt}})$ for the optimal choice of α . From the discussion in section 2.4, in particular Fig. 4, it should be clear that we could equally well have applied error propagation using the variances and the covariance of the two original estimators.

The analysis of a times series of U_{c} has the advantage that, for a more detailed discussion, the variance of the individual measurement and the autocorrelation time of the combined estimator can be computed as well. In Tables 3 and 4 we list for each estimator the variance $\sigma_{\text{k,v,c}}^2$ of the individual measurements as well as their integrated autocorrelation times $\tau_{\text{int,k,v,c}}$. As already mentioned, the reported errors for these quantities were obtained using jackknife blocking.

Looking at the energy values in Tables 1 and 2, the first thing we notice is that all three estimators give indeed compatible energy estimates within error bounds and all estimates converge to the correct continuum energy of $U = 0.80377$ (CP) resp. -0.903965 (DW). These values can be easily obtained by numerical integration of the associated Schrödinger equation. For the convex potential this is basically the ground-state energy E_0 , since already the first excited state with $E_1 = 2.736$ is strongly suppressed at $\beta = 10$ and does not affect the significant digits of U . For the double-well potential the value of U was obtained by using $E_0 = -0.913371$, $E_1 = -0.892348$, $E_2 = 0.029846$, and $E_3 = 0.37813$.

One also recognizes a distinct finite-size dependence which on theoretical grounds should be proportional to L^{-2} . For the most accurate measurements in our simulations (using the combined estimator and the W-cycle) we find that only for $L \geq 256$ (CP) resp. $L \geq 128$ (DW) the discretization error is no longer relevant. We mention in passing that this systematic error may be reduced using the Takahashi-Imada scheme³¹ based on higher-order Trotter decomposition. Since this modification only amounts to adding a local term to the potential energy this scheme is perfectly compatible with all update

algorithms discussed here, and as far as the qualitative behaviour of statistical errors is concerned we do not expect any significant deviations from the conclusions drawn in this study.

5.3 Autocorrelation times and statistical efficiency

The integrated autocorrelation times for the two potentials and the four update algorithms collected in Tables 3 and 4 are plotted in Figs. 6(a)-(h) against L on a double-logarithmic scale. As discussed in section 2.3 and illustrated in Fig. 1, the variance does not depend on the update algorithm but it strongly depends on the estimator. As we will see, the different dependencies of the variance and the autocorrelation times on the number of variables L combine in a peculiar way in the errors $\Delta \equiv \Delta \bar{U}$ which are plotted in Figs. 7(a)-(h). Comparing the “kinetic” and the “virial” estimators, the combination often leads to a crossover for the final error. The error of the combined estimator is, however, always smaller than the better of the two estimators.

Metropolis algorithm: In Figs. 6(a) and (b) we observe for the autocorrelation time of the virial estimator the expected quadratic divergence. By fitting the power-law ansatz $\tau_{\text{int}} = \alpha L^z$ to the data for the convex potential (CP) with $L = 128, 256, 512$, and 1024 we obtain indeed an exponent of $z = 2.017(13)$. The autocorrelation times of the kinetic estimator in this case behave rather differently, and at first glance it may seem that they do not show the expected L^2 -divergence. It is clear, however, that the plotted fit with an “effective” exponent of $z = 1.372(16)$ is not really justified since there is still distinct curvature for the last three data points ($L = 256, 512, 1024$). For the double-well potential the difference between the two estimators is even more pronounced. For the virial estimator we obtain in the range $64 \leq L \leq 1024$ again an excellent fit with an exponent of $z = 1.986(54)$, which is fully consistent with the expected value of two. For the data of the kinetic estimator in the same range the quality of the fit is greatly reduced and the “effective” exponent of $z = 0.461(15)$ is again found to be much smaller. By successively discarding small values of L in the fit we observed a definite trend to larger values of z , but the available sizes of L are still much too small to see the truly asymptotic behaviour for the kinetic estimator.

We may, however, compare the autocorrelation times with those of the moments $m_2 \equiv \sum_{i=1}^L x_i^2$ and $m_4 \equiv \sum_{i=1}^L x_i^4$ reported in an earlier investigation,⁹ which are of the same order of magnitude. The same is true for the autocorrelation times of the correlations $x_k x_{k-1}$ which we have elsewhere found²⁴ for the convex potential to increase as 1.078(14), 1.903(22), 4.466(94), 13.53(70), 52.3(6.6), and 227(21) for lattices of size $L = 8, 16, 32, 64, 128$, and 256. Surprisingly enough, the autocorrelation times of the kinetic estimator are much smaller and start to diverge only much later. Recall that due to the periodic boundary conditions and translational invariance the kinetic estimator is a linear combination of m_2 , m_4 , and $x_k x_{k-1}$. The particular combination, however, has a much smaller autocorrelation time.

As a consequence, contrary to previous expectations, for the Metropolis algorithm the kinetic estimator turns out to be much more accurate than the virial estimator for the parameters under consideration. This is clearly seen in Figs. 7(a) and (b). Note, however, that this result depends crucially on the observed autocorrelation times in the range of L -values investigated here. If also for the kinetic estimator the autocorrelation times asymptotically diverge as $\tau_{\text{int},k} \propto L^2$, then we should find for very large L that $(\Delta \bar{U}_k)^2 \propto \sigma_k^2 \tau_{\text{int},k} \propto L^3$, while the error for the virial estimator exhibits a weaker L -dependence of $(\Delta \bar{U}_v)^2 \propto L^2$.

Since modified update algorithms such as the staging algorithm and the multigrid W-cycle eliminate slowing down the virial estimator for these update schemes will asymptotically *always* be more favorable.

Multigrid V-cycle: The different behaviour of the autocorrelation times for the kinetic and virial estimators is also found, albeit less pronounced, for the V-cycle. Fitting our data for $L = 256, 512$, and 1024 in Figs. 6(c) and (d) we find for the virial estimator exponents of $z = 0.959(54)$ (CP) and $z = 0.808(42)$ (DW), supporting the expected value of $z = 1$. The corresponding exponents for the moments m_2 of $z = 0.8356(92)$ (CP) and $z = 0.715(27)$ (DW), obtained elsewhere⁹ fitting data for $L = 128, 256$, and 512, are compatible with these values taking into account the fact that those data still showed some upward curvature and were hence conjectured to underestimate the asymptotic behaviour.

Again, however, the kinetic estimator has much smaller autocorrelation times. For $L \leq 1024$ the fits give here effective exponents of $z = 0.135(18)$

(CP) and $z = 0.078(23)$ (DW). Even though we can of course not exclude the possibility that the data again start to diverge much faster for larger values of L , our data do not show any tendency of upward curvature.

Taking into account the fact that also the variance for small values of L is much smaller for the kinetic estimator we find that, for small L , the actual errors for the kinetic estimator are much smaller as well. In Figs. 7(c) and (d) we see that with increasing L the difference decreases, and for $L \approx 50$ both estimators would roughly yield the same error. For large values of L the virial estimator gets still better but for values in the range $256 \leq L \leq 1024$ the errors for the two estimators seem to increase with roughly the same effective exponent.

Multigrid W-cycle: The W-cycle exhibits a considerably improved dynamical behaviour and the magnitude of the autocorrelation times shown in Figs. 6(e) and (f) is now greatly reduced to about unity. Notice that in contrast to all other update algorithms here the virial estimator has smaller autocorrelations than the kinetic estimator. In particular the divergence with increasing L is much weaker for both estimators. Only for the convex potential we still find a slight increase of the autocorrelation times for the virial estimator with an exponent of $z = 0.1087(65)$, while the corresponding exponent for the kinetic estimator, $z = 0.052(11)$, is compatible with zero. For the double-well potential both exponents ($z = 0.040(63)$ for the virial and $z = 0.028(12)$ for the kinetic estimator) are consistent with zero. Hence the continuum slowing down problem is solved for the W-cycle. Again these estimates are in good agreement with the corresponding exponents for the moments m_2 of $z = 0.1043(29)$ (CP) and $z = -0.015(11)$ (DW) obtained in our earlier investigation.⁹

Since the autocorrelation times no longer diverge and since the behaviour of the variances does not depend on the update algorithm, we expect a crossover for the actual errors associated with the virial and the kinetic estimator. Such a crossover was already observed for the V-cycle in Figs. 7(c) and (d), but for the W-cycle in Figs. 7(e) and (f) it is much more pronounced. Basically this simply reflects the behaviour of the variances σ_v^2 and σ_k^2 shown in Fig. 1, which exhibit a clear crossover around $L = 64$ for the convex and around $L = 100$ for the double-well potential, respectively. Since for large values of L the statistical errors of the virial estimator remain roughly con-

stant, it here always outperforms the kinetic estimator whose errors increase due to the linear L -dependence of the variance.

Staging algorithm: From Figs. 6(g) and (h) it is obvious that also the staging algorithm eliminates slowing down. Notice that for the staging algorithm the virial estimator has larger autocorrelations than the kinetic estimator, while for the W-cycle it is just the other way around.

It should be kept in mind, however, that the staging algorithm requires the choice of an optimal staging length j_{opt} . This problem was discussed elsewhere¹⁰ for the virial estimator by explicitly looking at the autocorrelation times as a function of the staging length. It was shown that the optimal choice scales with the number of variables L , and that the corresponding optimal acceptance rates stay roughly constant for different L . Here we extend this discussion and list in Table 5 the values of j_{opt} and the corresponding acceptance rates for both the virial and the kinetic estimator. We see that the rule of thumb of some fixed acceptance probability regardless of the estimators is rather misleading. In fact, while for the virial estimator the optimal value of j corresponds to an acceptance rate of about 55%, for the kinetic estimator the optimum is at about 85% – 90%.

It should be observed that for an optimal performance we had to use a different j_{opt} for the two estimators, i.e., used data from different simulations. For the convex potential and the largest grid of $L = 1024$ the kinetic estimator had the lowest autocorrelation time of $\tau_{\text{int,k}}^{\text{opt}} = 1.097(21)$ (cp. Table 3) for a staging length of $j_{\text{opt}} = 56$ with an acceptance rate of 90%. Measuring the energy, on the other hand, for $j = 176$ with an acceptance rate of 56%, as was best for the virial estimator, produced an autocorrelation time of $\tau_{\text{int,k}} = 1.483(37)$. The virial estimator, on the other hand, had its lowest autocorrelation time of $\tau_{\text{int,v}}^{\text{opt}} = 2.48(56)$ for $j_{\text{opt}} = 176$. Here the autocorrelation time is in fact more than doubled to a value of $\tau_{\text{int,v}} = 4.53(17)$ if the optimal staging length $j = 56$ for the kinetic estimator was used. This is nothing but yet another example of the subtle interplay between update algorithm and energy estimator which calls for some care when one aims at optimizing the efficiency of PIMC simulations.

A bad choice of the staging length – if only properly scaled with L – only affects the absolute value of the autocorrelation times.¹⁰ If the staging length increases linearly with L the corresponding autocorrelation times are roughly

constant and do not depend on L . This is confirmed by the data displayed in Figs. 6(g) and (h) where we plotted fits with exponents of $z = 0.008(17)$ (CP) and $z = -0.005(20)$ (DW) for the virial estimator, and with exponents of $z = -0.012(13)$ (CP) and $z = 0.005(12)$ (DW) for the kinetic estimator. All these exponents are fully consistent with zero and we conclude that the staging algorithm eliminates slowing down just as well as the multigrid W-cycle. Looking at the error of the energy estimation in Figs. 7(g) and (h), which contains also the L -dependence of the variance, we hence observe the very same crossover as we did for the W-cycle.

5.4 The combined estimator

If the choice between the two estimators were exclusive, one would have to conclude that the best estimator would depend on details of the simulation. As discussed in section 2.4, however, one can always combine the two estimators and can hence always obtain errors which are even smaller than the value for the better of the two estimators. Looking at the errors displayed in Figs. 7(a)-(h), one sees that for the convex potential the gain by combining the two estimators is best for very small values of L where α is outside the range $[0, 1]$ (cp. Tables 1 and 2). Another situation where the combination appreciably reduces the error occurs, for both potentials, if the actual errors of the two estimators are of the same magnitude.

As was already suggested by Fig. 4, for refined update algorithms and large values of L the optimal interpolation parameter is always close to 0 which reflects the fact that the virial estimator here always wins the race. For the Metropolis algorithm where no crossover occurs, the opposite is true. Here the optimal α for large L is close to 1. For medium values of L , in the crossover region for the V- and W-cycle and the staging algorithm, any values of α were obtained.

Let us take a look at the autocorrelation times for the combined estimator displayed in Figs. 6(a)-(h). For the Metropolis algorithm the autocorrelation times (scaling effectively with exponents $z = 1.413(21)$ (CP) and $z = 0.469(51)$ (DW)) are close to but not necessarily smaller than those of the kinetic estimator. For the V-cycle the autocorrelation times of the combined estimator ($z = 0.523(38)$ (CP) and $z = 0.388(33)$ (DW)) are appreciably larger than those of the kinetic estimator but smaller than those of the virial estimator. For the W-cycle ($z = 0.136(12)$ (CP) and $z = 0.0110(88)$ (DW))

and for the staging algorithm ($z = 0.021(17)$ (CP) and $z = 0.042(17)$ (DW)) the situation is just reversed. Here the combined autocorrelation times behave qualitatively as the ones for the virial estimator.

Regardless whether the autocorrelation times of the combined estimator are close to the smaller ones of either of the original estimators it always yields errors which are slightly smaller. The gain is most pronounced for very small lattices and in the crossover region.

The best gain in the reduction of the error by combining the two estimators was obtained for $L = 8$ and the Metropolis algorithm where the error of the better estimator was in fact reduced by a factor of 2. For $L = 64$, the double well and the V-cycle the errors of 0.31 for the kinetic and 0.30 for the virial estimator were still reduced by a factor of 1.5 to an error of 0.21. Note that this reduction would be equivalent to a factor of more than 2 for the actual computer time needed to obtain the same reduction by better statistics for the individual estimators.

Unfortunately, for most cases the gain by combining the estimators is much smaller. Realistically one may expect a gain of, say, 10% in the final error by the combination which may seem moderate a gain. It should be kept in mind, however, that such a 10% gain in the error corresponds to something like a 20% reduction of the computer run time needed to achieve the same error by a simply increasing the statistics. And we emphasize again that the reduction gained by combination of the estimators may be obtained *after* the simulation completely without extra cost.

We finally observe that Fig. 7(h) seems to contradict our claim that the combination of the two estimators *always* reduces the error of the better estimator. For the double well and the staging algorithm with $L = 16$ and 32, the error of the combined estimator indeed is larger than the error for the kinetic estimator. The reason is that here the data for the kinetic estimator were in fact obtained from the simulation optimized for the virial estimator. As pointed out above, the choice for the optimal staging length depends on the estimator. The values for the two estimators U_k and U_v reported in Tables 1 and 2 were obtained for the respective *optimal* staging length j_{opt} for each estimator (cp. Table 5). Clearly, the optimal staging length for the combined estimator would be different both from the j_{opt} for either the kinetic or the virial estimator. In fact, we are dealing with an optimization problem of two dimensions in the parameter space of j_{opt} and α . However, in practical applications the combination of the estimators would be done *after*

the simulation. Unfortunately, one has to decide beforehand which j_{opt} best be chosen and regardless whether one might use $j_{\text{opt,k}}$ or $j_{\text{opt,v}}$, in either case one would use a non-optimal j_{opt} for one of the two estimators. In fact, if we would have measured the energy using the kinetic estimator U_k using the optimal staging length for the virial estimator, i.e. for $L = 16$ with $j = 6$ and for $L = 32$ with $j = 10$ we would have obtained values of $-0.9564(11)$ and of $-0.9184(20)$ respectively. Clearly, these values are no longer superior to the ones obtained using the combined estimator which were also computed for the optimal j for the virial estimator.

Thus, the apparent superiority of the kinetic estimator over the combined estimator in Fig.7 (h) is in fact an artifact of our over-careful data analysis. In practice, when the combination is done after the Monte Carlo run with data for the same set of parameters (non-optimal for at least one of the estimators), the combined estimator is guaranteed to yield the best energy estimates with the smallest error bars.

6 Conclusions

Our concern in this paper was to show how energy estimation in PIMC simulations can be optimized by taking into account both variances and autocorrelation times of two standard energy estimators: the “kinetic” and the “virial” estimator, and by investigating their respective interplay with different update algorithms: the standard *local* Metropolis algorithm, the *non-local* multigrid V- and W-cycles, and the *non-local* staging algorithm.

Let us briefly summarize the main points:

- (i) While the variance of the virial estimator depends only very weakly on the discretization scale, the variance of the kinetic estimator diverges asymptotically according to $\sigma_k^2 = L/2\beta^2$. This behaviour is independent of the update algorithm.
- (ii) The dynamics of the update algorithms affects the autocorrelation times of the standard estimators. For the Metropolis algorithm these diverge as L^2 but this behaviour can clearly be seen only for the virial estimator. In fact, the values of the autocorrelation times for the kinetic estimator turned out to be much smaller than those of the virial estimator, and we did not see the expected L^2 divergence with the

parameters in our simulations. Refined non-local update algorithms reduce (V-cycle) or eliminate (W-cycle, staging) an L divergence of the autocorrelation times. For the staging algorithm we observed quite a strong dependence of the autocorrelation times on the length of the staging segment. In particular, we have shown that the optimal length is very sensitive to the choice of the energy estimator. For both estimators it scales, however, linearly with L . In terms of acceptance rates the best performance was obtained at about 55% for the virial and about 85% – 90% for the kinetic estimator, respectively.

- (iii) The interplay between the variances of estimators and the dynamics of the update algorithms which affects the autocorrelation times turns out to be quite subtle. It furthermore also depends on the discretization parameter L . The kinetic estimator often has a smaller variance than the virial estimator for small L . Looking at the errors of the energy estimates we hence observe a crossover at which the virial estimator starts to win over the kinetic estimator since its variance does not increase with L . For the Metropolis algorithm, due to its small autocorrelation times for the kinetic estimator, the crossover point, however, is shifted to very large values of L and was not seen with the parameters in our simulation.
- (iv) As a simple solution to the involved interplay of the variance and the autocorrelation time for the two energy estimators we have introduced a “combined estimator.” By construction this *always* gives more accurate energy estimates than the better of the two standard estimators. The empirically observed gain varies but realistically one may expect a gain of about 10% in the error for energy estimation in PIMC simulations. We emphasize, that this corresponds to a 20% gain in actual simulation time which comes at no extra cost and is very easy to implement after the actual simulation.
- (v) The combination of different estimators for the same physical quantity is a very general option for Monte Carlo simulations and by no means restricted to the use of the standard energy estimators in PIMC simulations.

Acknowledgments

W.J. thanks the Deutsche Forschungsgemeinschaft for a Heisenberg fellowship.

References

- ¹H. De Raedt and A. Lagendijk, Phys. Rep. **128** (1985) 233; B.J. Berne and D. Thirumalai, Ann. Rev. Phys. Chem. **37** (1986) 401; J.D. Doll, D.L. Freeman, and T.L. Beck, Adv. Chem. Phys. **78** (1990) 61.
- ²J.A. Barker, J. Chem. Phys. **70** (1979) 2914.
- ³M. Creutz and B. Freedman, Ann. Phys. **132** (1981) 427.
- ⁴M.F. Herman, E.J. Bruskin, and B.J. Berne, J. Chem. Phys. **76** (1982) 5150.
- ⁵M. Parrinello and A. Rahman, J. Chem. Phys. **80** (1984) 860.
- ⁶A. Giansanti and G. Jacucci, J. Chem. Phys. **89** (1988) 7454.
- ⁷J.S. Cao and B.J. Berne, J. Chem. Phys. **91** (1989) 6359.
- ⁸W. Janke and T. Sauer, in: Proceedings of the international conference *Path Integrals from meV to MeV*, Tutzing, 1992, eds. H. Grabert, A. Inomata, L. Schulman, and U. Weiss (World Scientific, Singapore, 1993), p. 17.
- ⁹W. Janke and T. Sauer, Chem. Phys. Lett. **201** (1993) 499.
- ¹⁰W. Janke and T. Sauer, Chem. Phys. Lett. **263** (1996) 488.
- ¹¹All operators will be denoted by a “hat”, so that it is easy to identify whether a quantum statistical average $\langle \dots \rangle$ is to be understood in the operator or path-integral sense.
- ¹²H. Kleinert, *Path Integrals in Quantum Mechanics, Statistics and Polymer Physics*, 2nd edition (World Scientific, Singapore, 1995).
- ¹³Note that even though $\langle \frac{1}{L} \sum_{k=1}^L f(x_k) \rangle = \langle f(x_k) \rangle$ is trivially true for any function $f(x)$ due to the periodic boundary conditions in the path integral (5), the proper definition of estimators should always contain the summation over the path. This becomes crucial when considering the variance of the estimator which involves a term $\langle \left(\frac{1}{L} \sum_{k=1}^L f(x_k) \right)^2 \rangle \neq \langle f(x_k)^2 \rangle$.

- ¹⁴See, e.g., E. Merzbacher, *Quantum Mechanics*, 2nd edition (John Wiley, New York, 1970), p. 168.
- ¹⁵We would still have a valid energy estimator, though, as for any choice of α .
- ¹⁶With regard to the “best” estimate, given in Table 1.
- ¹⁷A.D. Sokal, *Bosonic Algorithms*, in *Quantum Fields on the Computer*, ed. M. Creutz (World Scientific, Singapore, 1992), p. 211.
- ¹⁸N. Madras and A.D. Sokal, J. Stat. Phys. **50** (1988) 109.
- ¹⁹W. Janke, *Monte Carlo Simulations of Spin Systems*, in *Computational Physics: Selected Methods – Simple Exercises – Serious Applications*, eds. K.H. Hoffmann and M. Schreiber (Springer, Berlin, 1996), p. 10-43.
- ²⁰W. Janke and T. Sauer, J. Stat. Phys. **78** (1995) 759.
- ²¹R.G. Miller, Biometrika **61** (1974) 1; B. Efron, *The Jackknife, the Bootstrap and other Resampling Plans* (SIAM, Philadelphia, PA, 1982).
- ²²N. Metropolis, S. Ulam, J. Am. Stat. Ass. **44** (1949) 335; N. Metropolis, A. W. Rosenbluth, M. N. Rosenbluth, A. H. Teller, and E. Teller, J. Chem. Phys. **21** (1953) 1087.
- ²³U. Wolff, Phys. Lett. **B288** (1992) 166.
- ²⁴T. Sauer, Ph.D. thesis, FU Berlin (1994).
- ²⁵J. Goodman and A.D. Sokal, Phys. Rev. Lett. **56** (1986) 1015; Phys. Rev. **D40** (1989) 2035; G. Mack, in *Nonperturbative Quantum Field Theory*, Cargèse 1987, eds. G. 't Hooft et al. (Plenum, New York, 1988), p. 309; G. Mack and S. Meyer, Nucl. Phys. **B** (Proc. Suppl.) **17** (1990) 293; D. Kandel, E. Domany, D. Ron, A. Brandt, and E. Loh, Jr., Phys. Rev. Lett. **60** (1988) 1591; D. Kandel, E. Domany, and A. Brandt, Phys. Rev. **B40** (1989) 330.
- ²⁶W. Hackbusch, *Multi-Grid Methods and Applications* (Springer, Berlin, 1985).

- ²⁷W. Janke and T. Sauer, Phys. Lett. **A197** (1995) 335.
- ²⁸W. Janke, *Recent Developments in Monte-Carlo Simulations of First-Order Phase Transitions*, in *Computer Simulations in Condensed Matter Physics VII*, eds. D.P. Landau, K.K. Mon, and H.-B. Schüttler (Springer, Berlin, 1994), p. 29.
- ²⁹W. Janke and T. Sauer, Phys. Rev. **E49** (1994) 3475.
- ³⁰E.L. Pollock and D.M. Ceperley, Phys. Rev. **B30** (1984) 2555; M. Sprik, M.L. Klein, and D. Chandler, Phys. Rev. **B31** (1985) 4234; *ibid.* **B32** (1985) 545; M.E. Tuckerman, B.J. Berne, G.J. Martyna, and M.L. Klein, J. Chem. Phys. **99** (1993) 2796.
- ³¹M. Takahashi and M. Imada, J. Phys. Soc. Jpn. **53** (1984) 963, 3765; X.-P. Li and J.Q. Broughton, J. Chem. Phys. **86** (1987) 5094.
- ³²Recall that for the Metropolis algorithm measurements were performed only every n_e sweep. Here we have rescaled the measured autocorrelation times to units of sweeps.
- ³³For a comparison of Figs. 7(a) and (b) with Tables 1 and 2 one has to keep in mind that the errors given in the tables refer to the full simulation with $n_e \times N_m$ sweeps, while in the figures we have rescaled them to hypothetical runs with $N_m = 100\,000$ sweeps (=measurements), i.e., the numbers in the tables have to be multiplied with $\sqrt{n_e}$ to obtain the data points in the figures.
- ³⁴This is, in fact, what we expect on general theoretical grounds.
- ³⁵For the Metropolis algorithm the autocorrelation times of the two estimators differ so much for $L \geq 128$ that it makes no sense to compute the combined estimator.

Convex Potential (CP): $V(x) = \frac{1}{2}x^2 + x^4$								
L	\overline{U}_k	%	\overline{U}_v	%	ρ	α_{opt}	\overline{U}_c	%
Metropolis								
8	0.48883(57)	0.12	0.4891(21)	0.43	0.913(58)	1.323	0.48874(29)	0.060
16	0.65741(86)	0.13	0.6553(23)	0.36	0.898(63)	1.120	0.65766(83)	0.13
32	0.7534(18)	0.24	0.7552(31)	0.42	0.86(11)	0.793	0.7537(17)	0.23
64	0.7864(37)	0.47	0.7783(58)	0.75	0.78(23)	0.825	0.7850(36)	0.46
128	0.8021(67)	0.84	0.788(11)	1.4	0.67(42)	0.863	0.8001(66)	0.83
256	0.8074(69)	0.86	0.791(11)	1.4	0.54(42)	0.933	0.8063(69)	0.86
512	0.8169(73)	0.89	0.817(10)	1.3	0.42(39)	0.819	0.8169(72)	0.88
1024	0.7990(96)	1.20	0.794(11)	1.4	0.30(38)	0.611	0.7973(86)	1.08
V-cycle								
8	0.48834(40)	0.082	0.4871(16)	0.33	0.912(49)	1.253	0.48866(25)	0.052
16	0.65847(57)	0.087	0.6581(16)	0.24	0.898(62)	0.969	0.65846(57)	0.087
32	0.7530(11)	0.15	0.7534(17)	0.23	0.857(73)	0.705	0.75313(81)	0.11
64	0.7916(23)	0.29	0.7864(18)	0.23	0.78(14)	0.391	0.7885(14)	0.18
128	0.8011(36)	0.45	0.7982(21)	0.27	0.67(23)	0.261	0.7990(18)	0.23
256	0.8085(58)	0.72	0.8051(26)	0.33	0.54(35)	0.170	0.8057(24)	0.30
512	0.8174(85)	1.04	0.8051(39)	0.48	0.42(38)	0.192	0.8075(34)	0.42
1024	0.807(13)	1.61	0.8008(56)	0.70	0.31(45)	0.164	0.8018(52)	0.65
W-cycle								
8	0.48844(32)	0.066	0.4882(13)	0.27	0.912(42)	1.228	0.48850(22)	0.045
16	0.65822(53)	0.081	0.6589(13)	0.20	0.898(59)	0.855	0.65831(49)	0.075
32	0.7537(13)	0.18	0.7521(14)	0.19	0.856(79)	0.546	0.75297(88)	0.12
64	0.7885(21)	0.27	0.7904(15)	0.19	0.78(12)	0.343	0.7898(12)	0.16
128	0.7924(33)	0.42	0.7963(14)	0.18	0.67(20)	0.192	0.7955(12)	0.15
256	0.8053(53)	0.66	0.8045(14)	0.17	0.54(30)	0.091	0.8045(13)	0.16
512	0.8102(76)	0.94	0.8050(14)	0.17	0.42(38)	0.032	0.8052(14)	0.17
1024	0.801(11)	1.38	0.8033(18)	0.22	0.31(39)	0.025	0.8032(18)	0.22
Staging								
8	0.48786(52)	0.11	0.4861(19)	0.39	0.913(53)	1.337	0.48845(25)	0.051
16	0.65907(67)	0.10	0.6594(20)	0.30	0.899(69)	1.121	0.65743(62)	0.094
32	0.7544(13)	0.17	0.7556(21)	0.28	0.858(90)	0.779	0.7546(12)	0.16
64	0.7902(20)	0.25	0.7889(23)	0.29	0.79(16)	0.411	0.7883(18)	0.23
128	0.7958(38)	0.48	0.7980(22)	0.28	0.67(26)	0.206	0.7990(19)	0.24
256	0.8051(50)	0.62	0.8025(27)	0.37	0.54(35)	0.101	0.8035(26)	0.32
512	0.7981(71)	0.89	0.8050(26)	0.32	0.41(48)	0.076	0.8035(25)	0.31
1024	0.799(11)	1.4	0.7968(22)	0.28	0.31(52)	0.047	0.7969(21)	0.26

Table 1: Convex Potential (CP): Measured energies using the kinetic estimator U_k , the virial estimator U_v , and the combined estimator U_c . Also listed are the relative jackknife errors in percent, the cross-correlation coefficient ρ , and the parameter α_{opt} of the optimal combined estimator.

Double Well (DW): $V(x) = -\frac{1}{2}x^2 + 0.04x^4$								
L	\overline{U}_k	%	\overline{U}_v	%	ρ	α_{opt}	\overline{U}_c	%
Metropolis								
8	-1.04785(70)	0.067	-1.0516(36)	0.34	0.88(13)	1.000	-1.04785(70)	0.067
16	-0.9547(12)	0.13	-0.9576(72)	0.75	0.84(32)	0.991	-0.9548(12)	0.13
32	-0.9210(25)	0.28	-0.916(12)	1.31	0.79(52)	1.022	-0.9211(25)	0.28
64	-0.9051(31)	0.35	-0.917(15)	1.64	0.73(56)	0.943	-0.9057(30)	0.91
128	-0.8931(81)	0.91	-0.905(12)	1.76				
256	-0.899(13)	1.42	-0.916(11)	1.17				
512	-0.886(22)	2.42	-0.916(15)	1.60				
1024	-0.889(19)	2.06	-0.909(13)	1.38				
V-cycle								
8	-1.04822(45)	0.043	-1.0484(26)	0.25	0.88(10)	1.012	-1.04822(45)	0.043
16	-0.95403(81)	0.085	-0.9555(23)	0.24	0.84(11)	0.883	-0.95421(76)	0.080
32	-0.9184(14)	0.15	-0.9196(23)	0.25	0.79(12)	0.714	-0.9187(12)	0.13
64	-0.9073(28)	0.31	-0.9080(27)	0.30	0.73(16)	0.488	-0.9077(19)	0.21
128	-0.9041(39)	0.44	-0.9060(33)	0.37	0.64(22)	0.418	-0.9052(25)	0.28
256	-0.9108(65)	0.72	-0.9053(38)	0.42	0.53(31)	0.248	-0.9066(33)	0.37
512	-0.9016(97)	1.08	-0.9080(63)	0.70	0.41(42)	0.327	-0.9059(48)	0.53
1024	-0.902(13)	1.45	-0.8918(80)	0.90	0.31(47)	0.274	-0.8945(67)	0.75
W-cycle								
8	-1.04776(39)	0.038	-1.0479(20)	0.19	0.876(81)	1.020	-1.04775(39)	0.038
16	-0.95539(79)	0.083	-0.9513(21)	0.22	0.84(19)	0.872	-0.95487(74)	0.078
32	-0.9179(15)	0.17	-0.9195(19)	0.21	0.79(12)	0.617	-0.9185(12)	0.13
64	-0.9104(29)	0.32	-0.9107(21)	0.23	0.73(13)	0.349	-0.9106(16)	0.18
128	-0.9054(34)	0.38	-0.9045(21)	0.24	0.64(18)	0.289	-0.9047(17)	0.19
256	-0.9036(57)	0.63	-0.9039(21)	0.24	0.53(23)	0.146	-0.9038(18)	0.20
512	-0.8979(75)	0.84	-0.9001(22)	0.25	0.41(30)	0.076	-0.9000(22)	0.25
1024	-0.8989(98)	1.09	-0.9061(24)	0.24	0.32(33)	0.073	-0.9056(19)	0.21
Staging								
8	-1.04841(65)	0.062	-1.0542(37)	0.35	0.88(13)	1.003	-1.04839(65)	0.062
16	-0.95318(91)	0.095	-0.9582(35)	0.37	0.84(16)	0.916	-0.9566(11)	0.11
32	-0.9189(15)	0.16	-0.9157(44)	0.48	0.79(20)	0.817	-0.9179(18)	0.20
64	-0.9053(26)	0.29	-0.9102(44)	0.48	0.73(26)	0.683	-0.9081(25)	0.28
128	-0.9013(37)	0.41	-0.9086(45)	0.50	0.64(27)	0.490	-0.9081(32)	0.35
256	-0.9011(55)	0.61	-0.8979(46)	0.51	0.53(33)	0.341	-0.9005(37)	0.41
512	-0.9178(80)	0.87	-0.9031(42)	0.47	0.42(35)	0.229	-0.9044(36)	0.40
1024	-0.907(11)	1.2	-0.8999(44)	0.49	0.31(52)	0.112	-0.9004(41)	0.46

Table 2: Double Well (DW): Measured energies using the kinetic estimator U_k , the virial estimator U_v , and the combined estimator U_c . Also listed are the relative jackknife errors in percent, the cross-correlation coefficient ρ , and the parameter α_{opt} of the optimal combined estimator.

Convex Potential (CP): $V(x) = \frac{1}{2}x^2 + x^4$						
L	σ_k^2	$\tau_{\text{int},k}$	σ_v^2	$\tau_{\text{int},v}$	σ_c^2	$\tau_{\text{int},c}$
Metropolis						
8	0.00916(13)	1.636(51)	0.1049(14)	1.825(48)	0.003440(28)	1.053(28)
16	0.01942(16)	1.758(51)	0.1272(18)	2.378(56)	0.02097(15)	1.535(32)
32	0.07641(58)	2.079(45)	0.1345(19)	4.44(14)	0.05683(53)	2.879(79)
64	0.2249(17)	2.619(81)	0.1278(30)	11.8(1.0)	0.1569(13)	3.40(14)
128	0.5418(43)	3.30(12)	0.1296(59)	47.6(9.6)	0.4055(34)	4.07(17)
256	1.1760(56)	6.03(15)	0.1285(48)	165(36)	1.0247(49)	6.47(17)
512	2.469(12)	13.91(24)	0.1311(42)	660(110)	1.6593(83)	15.97(29)
1024	5.015(23)	47.55(80)	0.1280(52)	3160(570)	1.8888(83)	65.9(1.9)
V-cycle						
8	0.00929(10)	0.845(15)	0.1059(11)	1.033(16)	0.003658(32)	0.6988(72)
16	0.01965(24)	0.746(11)	0.1297(20)	0.912(14)	0.01978(26)	0.732(11)
32	0.07632(46)	0.982(17)	0.1335(10)	0.909(18)	0.05284(35)	0.824(13)
64	0.2248(11)	1.163(22)	0.1352(13)	1.092(22)	0.08560(71)	0.947(18)
128	0.5450(32)	1.326(19)	0.1350(12)	1.583(31)	0.11181(83)	1.399(25)
256	1.1847(72)	1.460(25)	0.1352(15)	2.701(82)	0.1275(12)	2.321(65)
512	2.451(13)	1.638(30)	0.1372(22)	5.07(21)	0.1785(16)	3.062(90)
1024	5.014(28)	1.758(32)	0.1345(27)	10.80(94)	0.2299(24)	5.07(25)
W-cycle						
8	0.009041(81)	0.6434(93)	0.10449(96)	0.851(16)	0.003796(26)	0.5702(36)
16	0.01962(12)	0.652(11)	0.1292(12)	0.692(12)	0.02198(17)	0.5485(69)
32	0.07590(44)	0.902(12)	0.13406(93)	0.644(11)	0.05400(36)	0.5626(75)
64	0.2265(11)	1.033(18)	0.1362(10)	0.6278(66)	0.08669(57)	0.6098(72)
128	0.5454(29)	1.103(16)	0.13335(91)	0.660(14)	0.10754(73)	0.641(12)
256	1.1794(73)	1.222(19)	0.13640(85)	0.7119(93)	0.12236(94)	0.690(10)
512	2.460(13)	1.177(22)	0.1357(11)	0.781(12)	0.12951(97)	0.765(12)
1024	5.002(28)	1.250(25)	0.1348(12)	0.859(16)	0.1314(12)	0.845(14)
Staging						
8	0.00900(11)	1.398(49)	0.1032(12)	1.545(32)	0.003454(26)	0.9084(36)
16	0.01936(19)	1.396(35)	0.1275(13)	1.518(24)	0.02117(14)	0.7878(39)
32	0.07628(45)	1.086(21)	0.1347(16)	1.850(44)	0.05588(42)	1.287(32)
64	0.2270(15)	1.114(22)	0.1336(14)	1.960(44)	0.08546(75)	1.644(41)
128	0.5453(29)	1.115(23)	0.1357(16)	2.012(49)	0.1083(12)	1.885(47)
256	1.1881(66)	1.110(18)	0.1344(18)	2.119(67)	0.1209(15)	2.086(64)
512	2.448(13)	1.076(16)	0.1339(16)	2.079(53)	0.1281(15)	2.019(57)
1024	5.054(29)	1.097(21)	0.1319(17)	2.048(56)	0.1306(16)	1.983(54)

Table 3: Convex Potential (CP): Variances $\sigma_{k,v,c}^2$ and the integrated autocorrelation times $\tau_{\text{int},k,v,c}$ for the kinetic (k), virial (v) and combined (c) energy estimator.

Double Well (DW): $V(x) = -\frac{1}{2}x^2 + 0.04x^4$						
L	σ_k^2	$\tau_{\text{int},k}$	σ_v^2	$\tau_{\text{int},v}$	σ_c^2	$\tau_{\text{int},c}$
Metropolis						
8	0.01282(30)	1.833(76)	0.3645(40)	2.564(48)	0.00128(30)	1.834(76)
16	0.03257(41)	1.87(13)	0.3683(74)	5.88(24)	0.00322(41)	1.89(13)
32	0.1050(14)	2.68(20)	0.364(12)	18.7(2.1)	0.1096(14)	2.59(19)
64	0.2598(19)	3.206(82)	0.352(13)	64.4(9.4)	0.2327(17)	3.62(11)
128	0.5746(42)	3.75(20)	0.361(11)	243(21)		
256	1.217(11)	4.99(24)	0.3500(95)	909(67)		
512	2.498(19)	6.17(33)	0.358(13)	4407(570)		
1024	5.048(23)	10.68(34)	0.365(12)	14752(1600)		
V-cycle						
8	0.01247(18)	0.839(53)	0.3682(28)	0.752(18)	0.00124(19)	0.840(50)
16	0.03356(27)	0.918(17)	0.3636(29)	0.746(12)	0.00330(23)	0.842(13)
32	0.10508(68)	1.146(23)	0.3590(27)	0.784(12)	0.00840(57)	0.968(15)
64	0.2605(16)	1.290(27)	0.3538(26)	0.945(16)	0.1551(11)	1.021(18)
128	0.5830(35)	1.438(28)	0.3575(36)	1.338(25)	0.2250(17)	1.396(27)
256	1.2168(65)	1.598(37)	0.3550(41)	2.297(61)	0.2749(28)	2.057(57)
512	2.519(14)	1.814(41)	0.3561(58)	3.92(15)	0.4293(39)	2.498(65)
1024	5.037(30)	1.790(38)	0.3657(74)	7.19(43)	0.5731(65)	3.60(14)
W-cycle						
8	0.01215(13)	0.597(20)	0.3631(24)	0.5478(76)	0.00120(13)	0.598(20)
16	0.03415(24)	0.836(26)	0.3647(25)	0.5121(79)	0.00340(22)	0.709(22)
32	0.10389(63)	0.987(20)	0.3587(23)	0.5128(74)	0.00930(61)	0.639(13)
64	0.2618(14)	1.110(27)	0.3573(25)	0.5291(75)	0.1837(13)	0.5762(91)
128	0.5856(33)	1.191(22)	0.3630(28)	0.5377(72)	0.2323(17)	0.6266(88)
256	1.2157(67)	1.274(22)	0.3566(26)	0.5479(72)	0.2864(20)	0.5841(74)
512	2.504(14)	1.236(24)	0.3627(26)	0.5650(95)	0.3246(24)	0.5842(92)
1024	5.070(28)	1.287(23)	0.3564(24)	0.5920(76)	0.3345(22)	0.6360(84)
Staging						
8	0.01242(30)	1.323(29)	0.3631(38)	1.779(36)	0.01239(31)	1.325(29)
16	0.03330(34)	1.240(48)	0.3582(41)	2.059(44)	0.03242(43)	1.579(61)
32	0.10403(76)	1.120(23)	0.3628(49)	2.182(63)	0.08351(77)	1.575(43)
64	0.2606(16)	1.117(22)	0.3539(48)	2.335(64)	0.1568(14)	1.648(27)
128	0.5847(35)	1.145(23)	0.3582(49)	2.406(76)	0.2337(25)	2.017(49)
256	1.2242(67)	1.139(24)	0.3597(52)	2.456(87)	0.2980(32)	2.085(71)
512	2.520(14)	1.164(20)	0.3592(52)	2.366(64)	0.3473(36)	2.095(49)
1024	5.067(27)	1.150(20)	0.3610(49)	2.406(69)	0.3478(42)	2.224(59)

Table 4: Double Well (DW): Variances $\sigma_{k,v,c}^2$ and the integrated autocorrelation times $\tau_{\text{int},k,v,c}$ for the kinetic (k), virial (v) and combined (c) energy estimator.

L	$j_{\text{opt,k}}$	%	$j_{\text{opt,v}}$	%
Convex Potential (CP)				
8	2	64	2	64
16	4	49	2	82
32	4	73	4	72
64	4	90	10	68
128	10	86	24	55
256	16	90	44	55
512	24	93	88	55
1024	56	90	176	56
Double-Well (DW)				
8	2	71	2	71
16	4	63	6	47
32	4	80	10	49
64	8	84	20	52
128	16	80	40	54
256	32	82	80	54
512	64	84	160	54
1024	128	84	320	54

Table 5: Optimal staging lengths $j_{\text{opt,k}}$, $j_{\text{opt,v}}$ and acceptance rates for the kinetic (k) and the virial (v) estimators.

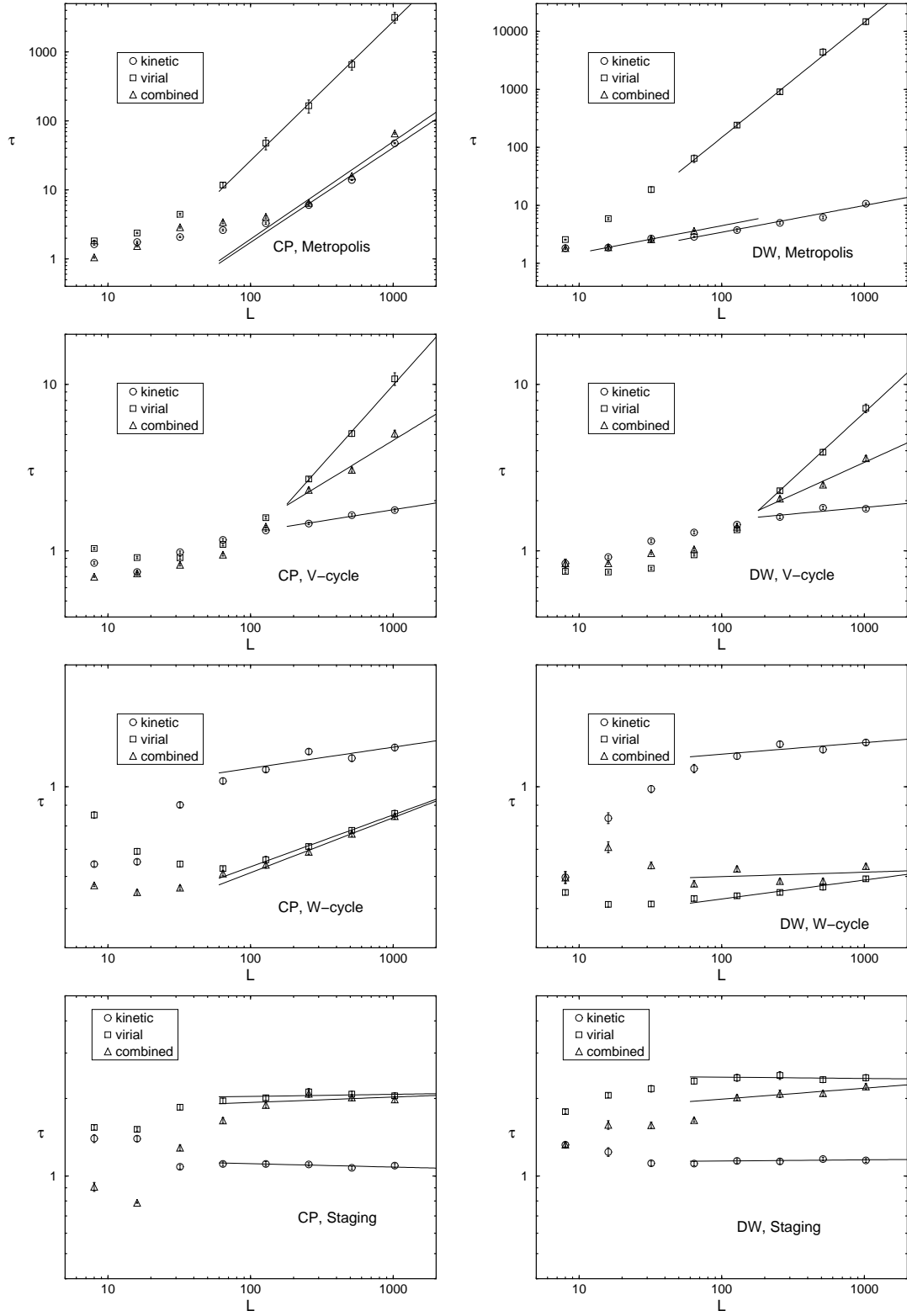


Figure 6: Integrated autocorrelation times τ_{int} on a logarithmic scale for the three energy estimators using different update algorithms for the convex potential (CP) and the double well (DW). Straight lines show fits of the form $\tau_{\text{int}} = \alpha L^z$.

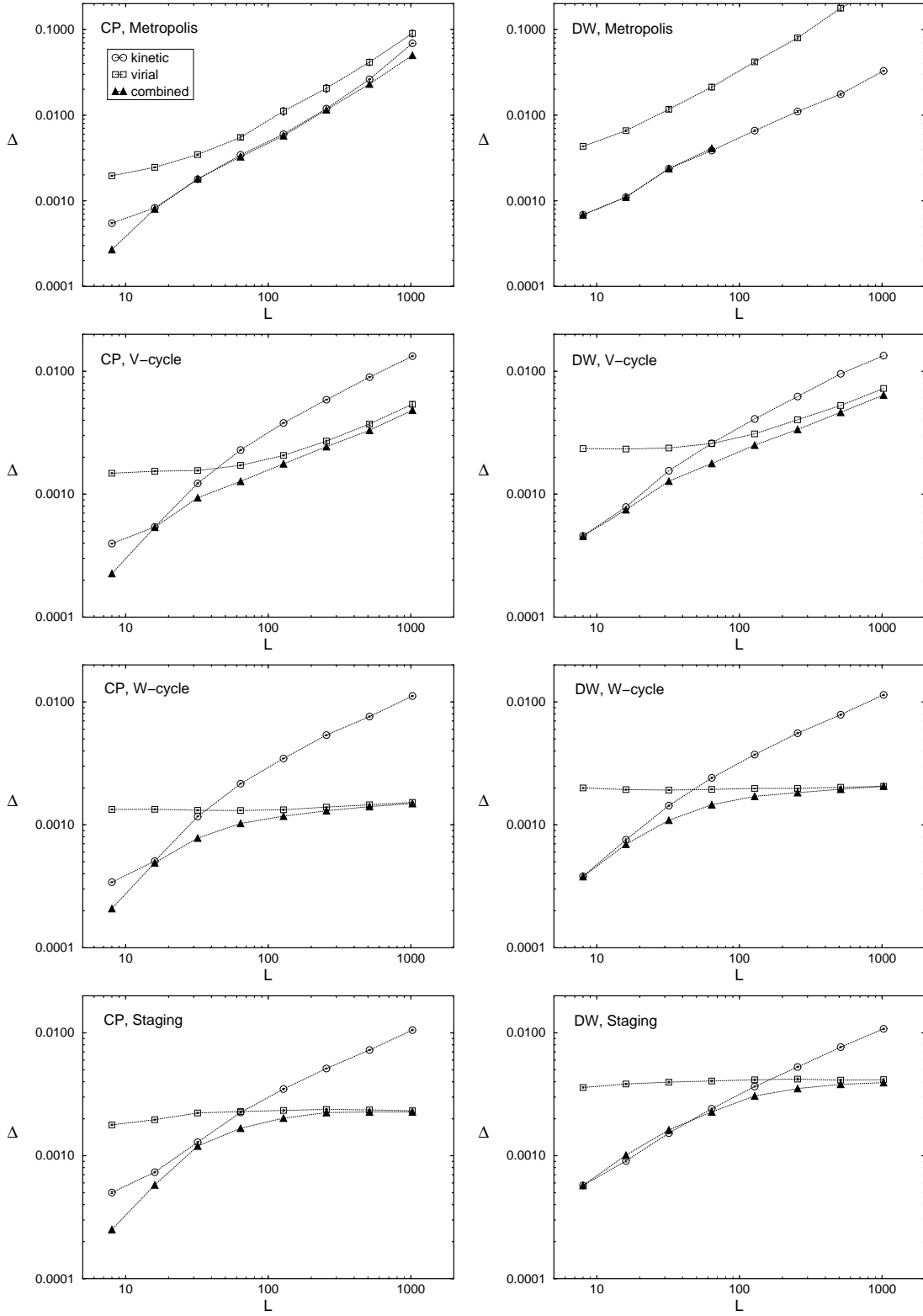


Figure 7: The errors $\Delta \equiv \Delta \bar{U}$ computed from the variance and the autocorrelation times for the three estimators using different update algorithms for the convex potential (CP) and the double well (DW).

Figure Captions

- Fig. 1:** Variance of the individual energy measurements using the “kinetic” and the “virial” estimators for the two potentials (6) and (7) at $\beta = 10$. While the variance of the virial estimator is roughly constant in the continuum limit $L \rightarrow \infty$, the variance of the kinetic estimator asymptotically diverges as $\sigma_k^2 = L/2\beta^2$.
- Fig. 2:** The optimal interpolation parameter α_{opt} as given in eq. (26) as a function of the ratio $\kappa = \Delta_v/\Delta_k$ and the correlation coefficient $\rho = \Delta_{kv}^2/(\Delta_k\Delta_v)$.
- Fig. 3:** The reduction factor R as given in eq. (27) as a function of the ratio $\kappa = \Delta_v/\Delta_k$ and the correlation coefficient $\rho = \Delta_{kv}^2/(\Delta_k\Delta_v)$.
- Fig. 4:** Relative statistical error $\Delta\bar{U}_c/\bar{U}_c$ of the linear combination \bar{U}_c of the two energy estimators for the convex potential as a function of the interpolation parameter α (using the W-cycle update algorithm). Data symbols denote jackknife averages over 100 blocks, and the solid lines are computed according to the theoretical prediction (23), using as input only the (jackknife) variances of the virial and the kinetic estimator (corresponding to $\alpha = 0$, resp. $\alpha = 1$) and the (jackknife) covariance of the two estimators. The arrows indicate the values of optimal α according to eq. (24).
- Fig. 5:** (a) The autocorrelation function $A(j)$ on a logarithmic scale and (b) the integrated autocorrelation time $\tau_{\text{int}}(k)$ of the virial estimator as obtained with the V-cycle multigrid algorithm for the convex potential (CP) at $\beta = 10$ and $L = 512$. Solid lines show fits according to eq. (31) resp. (33). The asymptotic value of $\tau_{\text{int}}(k)$ quoted in Table 3 is $\tau_{\text{int},v} = 5.07(21)$.
- Fig. 6:** Integrated autocorrelation times τ_{int} on a logarithmic scale for the three energy estimators using different update algorithms for the convex potential (CP) and the double well (DW). Straight lines show fits of the form $\tau_{\text{int}} = \alpha L^z$.

Fig. 7: The errors $\Delta \equiv \Delta \bar{U}$ computed from the variance and the autocorrelation times for the three estimators using different update algorithms for the convex potential (CP) and the double well (DW).